Carbohydrate Polymers 285 (2022) 119238

Contents lists available at ScienceDirect

Carbohydrate Polymers

journal homepage: www.elsevier.com/locate/carbpol

# Editing of the *starch synthase IIa* gene led to transcriptomic and metabolomic changes and high amylose starch in barley

Qiang Yang [a,b,1], Jinjin Ding [a,b,1], Xiuqin Feng [a,b,1], Xiaojuan Zhong [a,b], Jingyu Lan [a,b], Huaping Tang [a,b], Wendy Harwood [c], Zhongyi Li [d,2], Carlos Guzmán [e], Qiang Xu [a,b], Yazhou Zhang [a,b], Yunfeng Jiang [a,b], Pengfei Qi [a,b], Mei Deng [a,b], Jian Ma [a,b], Jirui Wang [a,b], Guoyue Chen [a,b], Xiujin Lan [a,b], Yuming Wei [a,b], Youliang Zheng [a,b], Qiantao Jiang [a,b,*]

[a] *State Key Laboratory of Crop Gene Exploration and Utilization in Southwest China, Sichuan Agricultural University, Chengdu, Sichuan 611130, China*
[b] *Triticeae Research Institute, Sichuan Agricultural University, Chengdu, Sichuan 611130, China*
[c] *John Innes Centre, Norwich Research Park, Norwich NR4 7UH, UK*
[d] *CSIRO Agriculture and Food, Black Mountain, Canberra, ACT 2601, Australia*
[e] *Departamento de Genética, Escuela Técnica Superior de Ingeniería Agronómica y de Montes, Edificio Gregor Mendel, Campus de Rabanales, Universidad de Córdoba, Córdoba 14071, Spain*

ARTICLE INFO

*Keywords:*
*Hordeum vulgare*
*Starch synthase IIa*
CRISPR/Cas9
Resistant starch
Starch properties
Metabolic pathway

ABSTRACT

In this study, a range of barley allelic mutants lost ADPG binding structure of *starch synthase IIa* (*SSIIa*) were created through targeted mutagenesis of *SSIIa* by RNA-guided Cas9. The transcriptomic and qRT-PCR results showed the increased mRNA expression of *HvGBSSI* and the decreased *HvSSIIa* and *HvSBEI* levels in *ssIIa* mutant grains, which were consistent with the expressions of GBSSI, SSS and SBE enzymatic activities, respectively. However, the increased expressions of *HvSSI* cannot effectively compensate for the loss of *HvSSIIa*. The metabolic pathway analysis showed that the mutation of SSIIa led to increased ADP-glucose synthesis in barley grains. The *ssIIa* mutant grains had two and six times amylose, and RS contents in control grains, respectively, and significantly changed starch structure and functions compared to the controls. No metabolite changes could compensate for the decrease of starch biosynthesis in the *ssIIa* null mutant.

## 1. Introduction

Barley (*Hordeum vulgare* L.) is the world's fourth most important cereal after wheat, rice, and maise. It can grow well even in harsh environmental conditions and thrive on marginal lands. The main uses of barley grains are as livestock feed and raw material for malting and brewing. More recently, attention has turned to dietary fibre, β-glucan, tocols, biologically active constituents, lowering blood cholesterol, and regulating glycemic index. The presence of high amounts of barley is used as a component of a healthy diet for human consumption due to its nutritional benefits and health effects. However, the low resistant starch (RS) content in barley grains limits its applications for functional and healthy food (Briggs, 2012).

Starch, the major dietary source of carbohydrates for humans, accounts for ~50% to 60% of the endosperm of barley and is the major storage polysaccharide of barley grains like other cereal grains. Barley starch comprises ~25% amylose and ~ 75% amylopectin; it is known that the quality of barley-based products can be much affected by starch properties (Fan, Guo, et al., 2017; Li et al., 2011). For example, high-amylose starch with a high amylose/amylopectin ratio can be used for producing RS suitable for a diabetic diet. Amylose-free starch with a low amylose/amylopectin ratio shows excellent freeze-thaw stability and is good for the frozen foods industry (Bird et al., 2000; Jane et al., 2010). A daily diet with high amylose content (AC)/RS is good for human health (Topping et al., 2003). However, AC/RS in barley cultivars is low, and it is hard to overcome this by traditional breeding methods (Zhu, 2017). An accepted genetic mechanism to increase AC/RS in cereals is suppressing the activity of genes involved in amylopectin synthesis (Li et al.,

* Corresponding author at: Triticeae Research Institute, Sichuan Agricultural University, Chengdu, Sichuan 611130, China.
*E-mail address:* qiantaojiang@sicau.edu.cn (Q. Jiang).
[1] These authors contributed equally to this paper.
[2] Retired.

https://doi.org/10.1016/j.carbpol.2022.119238
Received 20 September 2021; Received in revised form 7 January 2022; Accepted 6 February 2022
Available online 10 February 2022

2011).

In barley, enzymes involved in starch biosynthesis include ADP-glucose pyrophosphorylase (AGPase), granule-bound starch synthase (GBSS), soluble starch synthase (SSS), starch branching enzyme (SBE), and debranching enzyme (DBE) like other cereals (Li et al., 2011). AGPase is devoted to the first committed step in chloroplasts/chromoplasts and storage starch in amyloplasts. GBSS is the key enzyme for amylose synthesis (Nelson & Rines, 1962). GBSSI functions in the endosperm and pollen tissues and GBSSII functions in leaves and photosynthetic tissues; there is no genetic evidence that any other gene is essential for amylose synthesis. For amylopectin synthesis, SSS, SBE, and DBE are essential (Fan, Zhu, et al., 2017; James et al., 2003). Three SBEs (SBEI, SBEIIa, and SBEIIb) in cereals have been reported, and the relative expression quantities of these genes are significantly variable in different species. In barley endosperm, the expression levels of *SbeIIa* and *SbeIIb* is similar, which is different from other cereal species (Sun et al., 1998). Mutants in barley altered in *SBEIIa*, *SBEIIb*, or both have been induced using RNA interference. The phenotype of mutants with different genotypes were examined to study the roles of *SBEIIa* and *SBEIIb* genes in controlling the content and branching frequency of amylose and amylopectin in barley endosperm (Regina et al., 2010). *Starch synthase IIa* (SSIIa), one of the SSS genes encoded by the *SSIIa* (*SSII-3*) gene, is a locus on chromosome 7H. SSIIa converts ADP-glucose to starch polymers in the cereal endosperm by elongating short amylopectin chains to intermediate length (Fontaine et al., 1993; Luo et al., 2015). Altered *SSIIa* can obviously change the amylopectin content in cereals (Umemoto et al., 2004; Yamamori et al., 2000; Zhang et al., 2004). Loss of *SSIIa* activity leads to informative phenotypes in barley (Morell et al., 2003). A significant increase in amylose synthesis, a shortened amylopectin chain length distribution, a reduced gelatinisation temperature, and abolished the binding of SSI, SBEIIa, and SBEIIb to the starch granules, but no obviously changing in expression levels in the soluble fraction. The barley *ssIIa* null mutant BARLEYmax with high resistant starch content is already commercialised and distributed all over the world. Numbers of experimentation on animals indicated that Barleymax is good for animal health (Aoe et al., 2019; Bird, Flory, et al., 2004; Bird, Jackson, et al., 2004). The starch composition and properties of *ssIIa*-null barley mutants have been systematically analysed. However, a systematic analysis of gene transcription, metabolism, and activity of enzymes related to starch biosynthesis of *ssIIa*-null mutants is still lacking.

The CRISPR/Cas9 system is a valuable tool for generating site-specific mutations in genes of interest. For inducing site-specific mutant plants, a gene-editing construct is transformed into the genome of the donor plant, containing the *Cas9* gene and guide RNA expression cassettes, together with other elements necessary to generate transgenic plants. Indels are induced in the mutant plants by DNA nonhomologous end-joining repair after chromosomal DNA cleavage at the target site. Homozygote mutants can be identified in progenies of mutant plants by genotyping analysis. The CRISPR/Cas9 system has made it easier to realise targeted mutagenesis. It is an effective technology for studying the function of endogenous genetic factors in cereals (Xu et al., 2021; Huang et al., 2020; Zeng et al., 2020). However, no study has yet reported producing high AC/RS barley using genome editing technology.

A previous study has verified the negative correlation between SSIIa and amylose biosynthesis in multiple species. However, the vast difference in the genetic backgrounds of mutants induced by chemical mutagenesis may also contribute to the changes of the phenotypes. Mutants created by genome editing technology with the same genetic background are the best choice to verify the truth of the inference.

In this study, barley *SSIIa* allelic mutants were induced by RNA-guided Cas9. *SSIIa*-null mutants had a significant increase in amylose and RS contents, a higher resistance to digestion, and a noticeable change in starch chain length distribution, crystalline structure, and grain morphology. Various compositional parameters and starch properties of these mutants were analysed to verify the effects of *SSIIa* on barley starch biosynthesis.

## 2. Materials and methods

### 2.1. Barley materials

Barley cv. “Golden Promise” was used as the transgenic donor plant. The grown conditions of barley plants were controlled at 20 °C under a 16 h light/8 h darkness regime. Immature embryos with sizes from 1.5 to 2.0 mm in diameter were chosen for *Agrobacterium tumefaciens*-mediated transformation.

### 2.2. Plasmid construction and barley transformation

For cloning the coding region of the barley *SSIIa* gene, the genomic DNA of Golden Promise was extracted using the cetyltrimethylammonium bromide (CTAB) method described by Bekesiova et al. (1999). Three pairs of primers named SSIIa-$F_x$ and SSIIa-$R_x$ (x representing numbers 1–3; Supplementary Table 1) were designed. The coding region of *SSIIa* includes nine exons and eight introns, and the sequence from the initiation codon to the termination codon was 7102 bp long. Three single guide RNAs (sgRNA1, sgRNA2, and sgRNA3) targeting the second, eighth, and ninth exons were selected based on the web-based software (http://crispr.dbcls.jp). Following the manufacturer's instructions of the Plant Cas9/gRNA Plasmid Construction kit (catalog no. VK005-05; Viewsolid Biotech, Beijing, China), each of the three sgRNAs was separately ligated into vector pVK005 to generate genome-editing vectors pVK005-SS1 to pVK005-SS3 harbouring a single sgRNA (Fig. 1A and B). The plasmid of each genome-editing vector was introduced into *A. tumefaciens* strain $AGL_1$ competent cells. Positive clones were screened and used for *Agrobacterium*-mediated transformation of barley.

Barley transformation was conducted as described by Hinchliffe and Harwood (2019). The procedure performed for barley transformation was described in detail previously (Yang et al., 2019).

### 2.3. Screening for positive transgenic plants

The genomic DNA of transgenic barley plants and Golden Promise donor plants were extracted from barley leaf tissue using the CTAB method (Bekesiova et al., 1999). Primers, Hyg-F and Hyg-R, were used for amplifying the *hptII* gene to detect the presence of T-DNA from genome-editing vectors (Supplementary Table 1). The polymerase chain reaction (PCR) parameter was performed according to the instructions of 2× Long Taq PCR Master Mix (MT207-01; Biomed, Beijing), the PCR reaction parameters were 94 °C for 2 min; followed by 35 cycles of 10 s at 94 °C, 10 s at 60 °C, and 1 min at 72 °C; and a final extension at 72 °C for 5 min, with a hold step at 12 °C. The plasmid DNAs of the corresponding genome-editing vectors and the genomic DNA of Golden Promise were used as positive and negative controls. The PCR products were resolved on a 1.0% agarose gel at a voltage of 100 V.

### 2.4. Screening for mutant plants

All *hptII*-positive transgenic plants were identified as potential mutant individuals. Pooled genomic DNAs of each plant were extracted from leaf tissue sections consisting of an equal mass of leaves from each tiller using the BIOFIT Plant genomic DNA Extraction Kit (Baifeite, Chengdu, China). Primer pairs, sgRNAx-F/R (x representing numbers 1–3; Supplementary Table 1) were designed to amplify the corresponding target site in each transgenic $T_0$ plants. PCR was performed with high-fidelity polymerase DNA polymerase P505-d1 (Vazyme, Nanjing, China). Each PCR reaction contained about 100 ng pooled genomic DNAs, 12.5 μL 2× Phanta Max Buffer[a], 0.5 μL dNTP Mix (10 mM each), 10 μmoL primer F and R, 0.5 μL Phanta Max Super-Fidelity

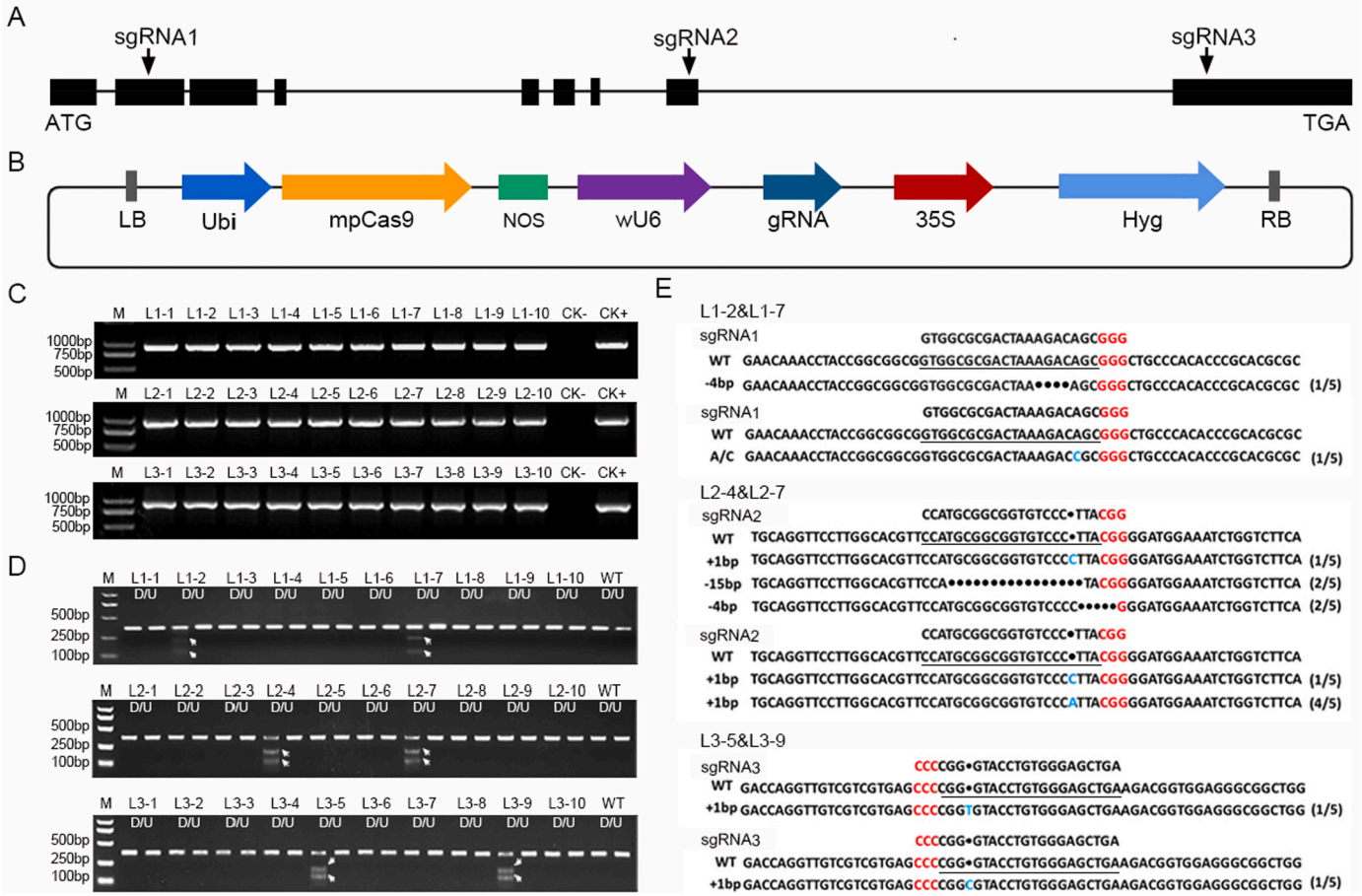


**Fig. 1.** Schematic diagram of the genome-editing vector and identification of $T_0$ mutant lines of barley *ssIIa* mutants.
(A) Genetic structure of the barley *SSIIa* gene and locations of sgRNA target sites. Solid boxes represent the exons, lines represent the introns, and arrows indicate the locations of sgRNAs. (B) Diagram of the pVK005 gene-editing vector. LB, left border; Ubi, maise ubiquitin 1 gene promoter; mpCas9, monocotyledon preferential codon-optimised Cas9; wU6, wheat U6 snRNA gene promoter; gRNA, guide RNA; 35S, cauliflower mosaic virus 35S promoter; Hyg, *hptII* selection marker gene; RB, right border. (C) PCR analysis (for *hptII* gene) of the surviving $T_0$ plants. CK+, plasmid DNA of the corresponding gene-editing vector; CK−, genomic DNA of Golden Promise. L1-1 to L1-10, L2-1 to L2-10, and L3-1 to L3-10 represent the transgenic lines from the sgRNA1, sgRNA2 and sgRNA3, respectively. (D) Enzymatic detection of mutations in $T_0$ lines transformed with the constructs of pVK005-SS1 (top), pVK005-SS2 (middle), and pVK005-SS3 (bottom). M, DNA ladder; D, digested PCR products of samples using endonuclease I; U, PCR products without enzyme digestion; WT, Golden Promise. White arrows indicate the bands resulting from enzyme digestion. L1-1 to L1-10, L2-1 to L2-10, and L3-1 to L3-10 represent the transgenic lines from the sgRNA1, sgRNA2 and sgRNA3, respectively. (E) Genotype analyses of $T_0$ mutant lines. Letters in red represent the PAMs. Letters in blue represent the insertions, and dots represent the deletions of the nucleotides. The numbers before bp at the left sides of the mutated sequences indicate the differences between the mutants and WT. The numbers in the brackets at the right sides of the mutated sequences indicate the frequencies of the mutated sequences. (For interpretation of the references to colour in this figure legend, the reader is referred to the web version of this article.)

DNA Polymerase, made up a total volume to 25 μL with sterile water. The PCR parameters were set with 1 cycle of 95 °C for 3 min, 35 cycles of 95 °C for 15 s, and annealing for 15 s at $T_m$ (marked in Supplementary Table 1), 72 °C for 30 s; and a final extension at 72 °C for 5 min, with a hold step at 16 °C. After the resolution of products on a 1% agarose gel, the PCR product was extracted and purified using the E.Z.N.A.™ Gel Extraction kit (Omega, Norcross, GA, USA).

The endonuclease I enzyme digestion reaction was carried out following an annealing reaction with a purified PCR product. The annealing reaction contained about 400 ng purified PCR product, 2 μL 10× endonuclease I reaction buffer, made up a total volume to 19 μL with sterile water. The annealing parameters were set with 95 °C for 5 min, then a 2 °C decrease per second from 95 °C to 85 °C, a 0.1 °C decrease per second from 85 °C to 25 °C, and finally, a cooling process was carried out before a hold step at 4 °C. For the digestion reaction, the annealed PCR product was equally divided into two Eppendorf tubes, one for enzyme digestion and the other one as negative control. 1 μL endonuclease I or sterile water were added into the reaction or control tube, respectively. Incubating the tubes at 37 °C for 15 min. The enzymatic digestion parameters have been reported in detail previously (Yang et al., 2020). Finally, the enzymatically digested products were resolved on a 2% agarose gel at a voltage of 65 V. The genomic DNA of Golden Promise donor plants was used as a negative control.

The targeted region was cloned for each positive mutant plant identified with endonuclease I enzyme digestion. Five clones derived from each positive mutant plant were randomly selected for sequencing. The sequencing results were then aligned with the sequences of Golden Promise to analyse the mutation types of the positive mutant plants.

### 2.5. Genetic analysis of potential off-target sites

The web-based software (http://crispr.dbcls.jp) was used to analyse the putative off-target sites for each genome-editing target site with the conditions required in a previous study (Yang et al., 2020). Primer pairs, F/R-sg$_X$-tb$_Y$ (X representing sgRNA numbers and Y representing the putative off-target numbers of each target site; Supplementary Table 1), were designed to amplify the corresponding off-target site. The conclusion for no off-target at the putative off-target site was obtained

only when there were no mismatched DNA sequences from 10 colonies for one mutated site compared to the DNA sequence of wild-type (WT) Golden Promise donor plants.

### 2.6. Sodium dodecyl sulfate-polyacrylamide gel electrophoresis (SDS-PAGE)

The proteins were extracted from halves of the barley grains following the published extraction process (Yamamori et al., 1994). Grain powder was ground from the endosperm part of the barley grains and transferred into a 1.5 mL Eppendorf tube. Solution I (700 μL) containing 55 mM Tris-HCl (pH 6.8), 2.3% SDS, 5% β-mercaptoethanol, and 10% glycerol was added and vortexed to wash the barley powder. The sample tube was centrifuged at 10,000 rpm at 4 °C for 5 min, and the supernatant was discarded. The washing program was repeated thrice. The sample was air-dried after the last wash and weighed accurately. Solution II (containing 55 mM Tris-HCl (pH 6.8), 2.3% SDS, 5% β-mercaptoethanol, 10% glycerol, 0.005% bromophenol blue), was added in a portion of 10 μL Solution II to 1 mg sample. The tube was vortexed, boiled for 5 min, and centrifuged at 12,000 rpm at 4 °C for 5 min (Wang et al., 2007). The supernatant (10 μL) was loaded onto 12% SDS-PAGE gel as described early (Yan et al., 2000). After electrophoresis, the gel was stained in the coomassie blue solution (containing 1.0% Coomassie blue-R250, 2.5% isopropyl alcohol, and 1% acetic acid) for 0.5 h and washed in MQ water for 3 times of 20 min. The gel was stained with a silver staining kit (Beyotime, Shanghai, China).

Every $T_1$ grain of the $T_0$ mutant plant was analysed, and all of the *ssIIa* null grains were germinated and transplanted for further studies. A certain number of $T_2$ progenies of each $T_1$ *ssIIa* null plant were randomly selected for SDS-PAGE analysis. The homozygous $T_1$ mutant plant was identified when all $T_2$ grains from the corresponding line had *ssIIa* null mutations. The proteins of nontransgenic Golden Promise grain were extracted and analysed by the same procedure as a reference.

### 2.7. Genotypic analysis of ssIIa-null plants

All $T_1$ *ssIIa*-null mutant grains identified by SDS-PAGE were planted. The genomic DNA of each plant was extracted and used as a template to amplify the targets region with primer pairs used for endonuclease I enzyme digestion analysis. The PCR products were sequenced to show the genotype of the corresponding $T_1$ mutant plant. The genotypes of $T_2$ *ssIIa*-null grains were analysed by the same procedure to check the transferring null mutations from $T_1$ to $T_2$ mutants.

### 2.8. Analysis of the presence or absence of T-DNA

Primers, Cas9-F and Ca9-R, were designed based on the sequence of the *Cas9* gene. PCR with the genomic DNA of $T_2$ plants used as a template was carried out to amplify the *Cas9* gene to verify the presence or absence of T-DNA. The PCR parameters were 94 °C for 2 min, followed by 30 cycles of 30 s at 94 °C, 30 s at 54 °C, and 1 min at 72 °C, and a final extension at 72 °C for 5 min, with a hold step at 16 °C. The PCR products were resolved by electrophoresis in a 1% agarose gel.

For further verification of the absence of T-DNA, the hygromycin resistance test was used to examine whether the *hptII* gene was still integrated with the barley genome. Healthy leaves (5 cm long) were cut from each $T_2$ plant. All the leaf segments were soaked in a solution (containing 40 mg/L hygromycin B and 1 mg/L 6-benzylaminopurine, pH 7.0). The leaf sections of Golden Promise at the same developmental stage were used as the negative control. The results were recorded by a camera when distinct colour differences occurred among individuals.

### 2.9. Measurement of grain morphologies of mutant barley grains

The $T_2$ mature grains of mutant and non-genome-edited (NE) plants were harvested and dried in an oven at 37 °C for 72 h. The 100 grain weight of each mutant and NE plant was measured, and the 1000 grain weight (TGW) was calculated. Two grains of each plant were chosen randomly to record the images of grains using an Olympus microscope digital camera (SZX2-ILLK; Olympus Corporation, Tokyo, Japan). Fifty grains of each plant were randomly selected to measure the grain parameters of mutant and NE lines using scanning equipment (Epson EU-88, Japan), and the results were analysed using WINSEEDLE.

### 2.10. Measurement of the content of total starch, amylose, and RS

The total starch, amylose, and RS contents of mutant and NE grains were measured using the Megazyme Total Starch Assay Kit (No. K-TSTA), Amylose Assay Kit (No. K-AMYL), and RS Assay Kit (No. K-RSTAR), respectively, according to the manufacturer's instructions (Megazyme, Ireland).

### 2.11. Starch extraction

The starch of mature barley grains was extracted and purified using a published procedure with minor changes (South & Morrison, 1990). Barley grains were soaked for more than 8 h in distilled water at 4 °C and crushed using mortar and pestle. The homogenate was transferred into a 2 mL Eppendorf tube and centrifuged at 4000 rpm for 5 min, and the supernatant was discarded. Distilled water (500 μL) and 80% (w/v) CsCl (1.5 mL) were added in turn to resuspend the sample. The sample tubes were then vortexed thoroughly and centrifuged immediately at 4000 rpm for 5 min, and the supernatant was discarded. The starch purification step was repeated with water and 80% CsCl. After washing the sample with washing buffer [55 mM Tris-HCl (pH 6.8), 2.3% (w/v) SDS, 1% (w/v) dithiothreitol, and 10% (v/v) glycerol] and acetone in turn, and they were dried with the lid open at room temperature. The samples were dissolved in dimethyl sulfoxide/LiBr solution and stored for a subsequent test.

### 2.12. Scanning electron microscopy (SEM), iodine staining and particle size analysis

The microstructure of purified starch granules from mutant barley grains were analysed by scanning electron microscope. ZEISS GeminiSEM 300 series (ZEISS, Germany) was used to perform this experiment. Starch granules from $T_2$ mature grains were fixed on circular aluminium stubs. Photos were taken by SEM at a voltage of 1.00 kV. The starch granules of Golden Promise and NE were used as controls. For iodine staining, starch granules were stained in potassium iodide stain (0.1% $I_2$, 1% KI) for 5 min and mixed with equal volume of glycerogelatin glycerinated gelatin (G1402, servicebio, Wuhan, China). One drop of mixture was dropped onto a microscopy slide by pipette, and photos were taken by optical microscopy (BX51, Olympus, Japan) under white light.

The starch granule size of the starch slurries was measured using Mastersizer 3000 (Malvern Instruments, Malvern, England) according to the manufacturer's instructions. The starch granules were divided into A- (>10 μm) and B-type (1–10 μm) according to the diameter, and the number and volume percentage of each type in mutants were calculated.

### 2.13. In vitro starch degradation analysis

The in vitro starch digestibility of mutant barley was analysed according to a published procedure with minor changes (Englyst et al., 1992). Starch (10 mg) and sterile water (500 μL) were premixed in a 2 mL Eppendorf tube. The sample was gelatinised in a boiling water bath for 20 min and transferred to a 37 °C water bath for a 20 min for the equilibrium of the temperature. An enzyme solution (1 mL) containing 20 mM sodium phosphate (pH 6.0), 6.7 mM NaCl, 0.01% $NaN_3$, 2.5 mM $CaCl_2$, and 4 units porcine pancreatic α-amylase (Sigma, A3176), and 4

U *Aspergillus niger* amyloglucosidase (Megazyme, E-AMGDF) was added and mixed. The sample tubes were then incubated in a shaker at 37 °C with 250 rpm shaking immediately. The enzymatic hydrolysis reaction solution (100 μL) was taken out after 20 and 120 min incubation, respectively. After sampling, 24 μL HCl (0.1 M) and 100 μL absolute alcohol were added and mixed to terminate the hydrolysis reaction immediately. The glucose content in each sample was measured using the D-Glucose Assay Kit (Ireland, Megazyme, K-GLUC). Finally, the glucose content was converted to the rapidly digestible starch (RDS), slowly digestible starch (SDS), and RS content according to the formula of Englyst et al. (1992). All samples were measured in triplicate, and the grains of NE plants were used as controls.

### 2.14. Analysis of starch chain length distributions

Fluorophore-assisted carbohydrate electrophoresis (FACE) carried out with the P/ACE MDQ Plus System (AB Sciex, USA) was used to analyse the highly accurate chain length distributions of amylopectin. The debranched starch sample (0.2 mg) was isolated and labelled with 1.5 μL 8-amino-pyrene-1,3,6,-trisulfonic acid (APTS) solution (5 mg APTS in 50 μL of 15% glacial acetic acid) and 1.5 μL sodium cyanoborohydride. The labelled sample was incubated in a bioshaker at 60 °C for 4 h in the dark. Deionised water (80 μL) was added to dissolve the sample through a low-speed vortex, and a 50 μL sample was transferred into FACE microvials for testing. The total peak areas from the degree of polymerisation (DP) of 6–70 (DP6–70) were used to normalise DP data with the reference data from the controls.

### 2.15. Determination of starch composition by size-exclusion chromatography (SEC)

The amylose and amylopectin content of barley starch was measured using an Agilent 1100 Series SEC System (Agilent Technologies, Waldbronn, Germany). Two analytical columns (GRAM 30 and 3000) and a refractive index detector (RID-10A; Shimadzu Corp., Kyoto, Japan) were used as auxiliary equipment. The experiments were performed according to the procedures described previously (Cave et al., 2009; Li et al., 2016). The molecular size distribution of branched starch was plotted as weight distribution, and the amylose and amylopectin contents were calculated.

### 2.16. Measurement of thermal properties

The gelatinisation of barley starch samples was analysed using a differential scanning calorimetry (DSC; DSC2920; TA Instruments, New Castle, DE, USA). Before the gelatinisation investigation, the barley starch sample was first mixed with distilled water in a ratio of 1:2 (w/w). For each sample, a 40 to 50 mg mixture was weighed accurately, sealed in a stainless-steel pan and then equilibrated at room temperature for more than 1 h. DSC measurements were performed following the parameter with a 10 °C increase per minute and varying in radians from 20 °C to 140 °C. All measurements for each barley starch sample were performed in triplicate, and an empty stainless-steel pan was treated with the same parameter as a reference. DSC thermograms were analysed using Universal Analysis 2000 version 4.3A (TA Instruments, Waters LLC, USA).

### 2.17. Solid-state $^{13}C$ cross-polarisation/magic angle spinning nuclear magnetic resonance (CP/MAS NMR) analysis

$^{13}C$ CP/MAS NMR was used to analyse the crystalline structure of *ssIIa*-null barley samples. Before the measurement, the test samples were packed in a holder and stored in a desiccator at a constant atmosphere [relative humidity (RH) of 75%] at 25 °C for 1 week. A saturated NaCl solution was used to maintain the RH. $^{13}C$ CP/MAS NMR experiment was conducted using a Bruker Avance III 400 WB spectrometer with resonance frequencies controlled at 100.6 MHz. The samples were packed in a 7 mm $ZrO_2$ rotor and spun at the magic angle (54.7°) with a 6 kHz spin rate. The CP/MAS ($^1H$-$^{13}C$) spectra were recorded with the contact time at 1.2 ms and recycle delay at 2 s, respectively. The chemical shifts were referenced to tetramethylsilane at 0 ppm. Typically, 8000 to 12,000 transients were accumulated for $^{13}C$ spectra (Wei et al., 2010).

### 2.18. Structure-function analysis of SSIIa protein

The online web-based software SMART (http://smart.embl-heidelberg.de/) was used to analyse the structure-function of SSIIa protein (Schultz et al., 2000). The barley *SSIIa* gene was translated into amino acid sequence using DNAman. Upload the SSIIa protein sequence into the data import window of SMART in FASTA format. Genomic mode was selected to analyse the structure-function of SSIIa, and the confidently domains, repeats, motifs, and feature predicted by SMART were identified as subjects for further study. Finally, Pfam:Glyco_transf_5, Pfam:Glyco_transf_1, and Pfam:Glyco_transf_1_4 were considered as the key components affecting the function of the SSIIa protein. These structures were annotated in detail on SMART, Pfam:Glyco_transf_5 represents the catalytic domain of glycogen (or starch) synthases that use ADP-glucose as the glucose donor, Pfam:Glyco_transf_1 and Pfam:Glyco_transf_1_4 indicate that protein has the function of transfer UDP, ADP, GDP or CMP linked sugars to glycogen, fructose-6-phosphate, and lipopolysaccharides. All of them belong to the Starch synthase catalytic domain.

### 2.19. AGP, GBSS, SSS, SBE, and DBE enzymatic activity assay

The AGP, GBSS, SSS, SBE, and DBE enzymatic activity assay were performed using the Solarbio AGP Enzyme Activity Assay Kit (No. BC0430), GBSS Enzyme Activity Assay Kit (No. BC3295), SSS Enzyme Activity Assay Kit (No. BC1855), SBE Enzyme Activity Assay Kit (No. BC1860), and DBE Enzyme Activity Assay Kit (No. BC4250), respectively. The pre-frozen (−80 °C) immature barley grains 15 DAA (day after anthesis) were used to analyse the AGP, GBSS, SSS, SBE, and DBE enzymatic activity of mutant and NE grains according to the manufacturer's instructions (Solarbio Science & Technology, Beijing, China). All samples were measured in triplicate.

### 2.20. Gene expression analysis by mRNA-seq and qRT-PCR

Total RNA used for the RNA-seq assays was isolated from three independent replicates of baley grains 15 DAA in the L1-2, L2-7, L3-9, and NE. All the experiments were performed according to the manufacturer's instructions RNAprep Pure Plant Plus Kit (DP441, Tiangen, Beijing, China). RNA samples were detected based on the A260/A280 absorbance ratio with a Nanodrop ND-1000 system (Thermo Scientific, USA). Paired-end libraries were prepared using KAPA Library Quantification Kit Illumina® Platforms (KAPA Biosystems) following the manufacturer's instructions. The synthesised double stranded cDNA fragments were then purified with an AMPure XP system (Beckman Coulter, Beverly, MA, USA). The purified double-stranded cDNA was polyadenylated and adapter-ligated for preparation of the pairedend library. Adaptor-ligated cDNA and adaptor primers were used for PCR amplification. PCR products were purified (AMPure XP system) and library quality was assessed on an Qseq100 DNA Analyzer (Bioptic Inc.). Finally, sequencing was performed with an Novaseq6000 instrument by SanShu Biotechnology (Shanghai, China).

The threshold for corrected p-values was determined via the false discovery rate (FDR) (FDR $< 0.001$, $|\log2(\text{ratio})| \geq 1$), and the criteria for identifying DEGs followed those of previously described methods, with several modifications. All the DEGs were annotated by Gene Ontology (GO) annotation terms and Kyoto Encyclopedia of Genes and Genomes (KEGG) pathways. The GO term and KEGG pathway analysis results were considered significant when the Bonferroni (Q-value)-

corrected p-value was ≤0.05. The enriched KEGG pathways were determined using R software.

The transcripts of genes related to starch biosynthesis were selected for validating the RNA-Seq data by real time polymerase chain reaction (qRT-PCR). Both the *ACTIN* and *GAPDH* genes were used as reference. Primers were designed and listed in Supplementary Table 1. Total RNAs were returned by SANSHU company, and the cDNAs were synthesised by HiScript II reverse transcriptase kit (R223, Vazyme, Nanjing, China) following the instructions. For each reaction tube, 1 μg total RNA, 4 μL 4 × gDNA wiper Mix, made up a total volume to 16 μL with RNase-free dd$H_2O$, hold the reaction tube at 42 °C for 2 mins. Then, 4 μL of 5 × HiScript II qRT SuperMix II were added and set up the reaction parameters at 50 °C for 15 min, 85 °C 5 s, with a hold step at 4 °C. At last, the cDNA-synthesised were diluted (1:10) with distilled water. The ChamQ Universa SYBR qPCR Master Mix kit (Q711, Vazyme, Nanjing, China) was used to perform the qRT-PCR. Each reaction contained 2 μL diluted cDNA, 0.8 μL (10 μM) primer F and R, 10 μL 2 × ChamQ Universa SYBR qPCR Master Mix, and 6.4 μL RNase-free dd$H_2O$. The PCR parameters were 1 cycle of 95 °C 30 s; 40 cycles of 95 °C 10 s, 60 °C for 30 s. The amplification and the data analysis were carried out in a Bio-Rad CFX96 Real-Time PCR Detection System (Bio-Rad Laboratories, Hercules, USA).

### 2.21. Untargeted metabolomics and energy-related metabolites analysis

Untargeted and energy-related metabolites were performed by San-Shu Biotechnology with LC-MS/MS. In brief, 100-mg barley grains 15 DAA of test samples were quickly frozen in liquid nitrogen immediately and grounded into fine powder with a mortar and pestle. The tissue samples with 100 μL of ice-cold $H_2O$ and five ceramic beads were homogenized using the homogenizer for 60s. 400 μL methanol/acetonitrile (1:1, v/v) were added to the homogenized solution for metabolite extraction. The solutions were sonicated for 30 min, and centrifuged at 14,000*g* for 15 min at 4 °C. The supernatants were transferred to clean plastic microtubes and dried with nitrogen; then the lyophilized powder was stored at −80 °C prior to analysis. Lyophilized samples were reconstituted by dissolving in 200 μL of 30% ACN. The samples were vortexed for 1 min and centrifuged at 14,000*g* for 15 min at 4 °C. The supernatants were collected for LC-MS/MS analysis using an UPLC Orbitrap-MS system (UPLC, Vanquish; MS, QE). Six technical replicates were performed for each test sample.

The raw MS data were acquired on the Q-Exactive using Xcalibur 4.1 (Thermo Scientific), and processed using Progenesis QI (Waters Corporation, Milford, USA). Quantified data were output into excel format. Data were analysed by R package, where it was subjected to multivariate data analysis, including principal component analysis (PCA) and orthogonal partial least-squares discriminant analysis (OPLS-DA). The 7-fold cross-validation and response permutation testing were used to evaluate the robustness ofthe model. The variable importance in the projection (VIP) value of each variable in the OPLS-DA model was calculated to indicate its contribution to the classification. Metabolites with the VIP value >1 was further applied to Student's *t*-test at univariate level to measure the significance of each metabolite, the p values less than 0.05 were considered as statistically significant.

### 2.22. Statistical analysis

All tests for grain morphologies, starch chemical composition, starch chemical structure, and other starch properties were performed on three $T_2$ progenies of each mutant line. The results were shown as the mean ± standard deviation (SD) in each mutant line. The differences between mutant lines and controls were analysed using IBM SPSS Statistics 21.

## 3. Results and discussion

### 3.1. Identification of transgenic positive and targeted $T_0$ mutant plants

Three *Agrobacterium*-mediated transformation experiments with constructs pVK005-SS1–SS3 were performed using immature barley embryos as the target tissue. Twenty, 36, and 13 $T_0$ plants were recovered, after selection on hygromycin B (40 mg/L), for constructs SS1-SS3, respectively. PCR amplification of the hygromycin gene showed that all surviving plants had a specific band with the same size as the positive control, gene-editing plasmid. In contrast, the transgenic donor plant Golden Promise used as negative control did not have any amplified band (Fig. 1C). The PCR results indicated that all $T_0$ plants selected had a T-DNA insertion, and the transformation efficiencies were 18.2%, 18.0%, and 21.7%, respectively (Table 1).

Six $T_0$ mutant plants were identified with nucleotide mutations at the corresponding gene-editing target sites using endonuclease I enzyme digestion. Two transgenic lines were recovered for each transformation experiment with sgRNA1, sgRNA2, and sgRNA3, respectively. To identify the mutations of these lines, the target region of each transgenic plant was amplified using the gene-editing target site-specific primers (Supplementary Table 1). For $T_0$ plants transformed with pVK005-SS1 to pVK005-SS3, the specific bands of 309, 315, and 349 bp were amplified from all 20, 36, and 13 surviving transgenic plants, respectively. After annealing and digesting the purified PCR products, $T_0$ plants L1-2 and L1-7 transformed with pVK005-SS1 were detected as positive mutants having two digested DNA bands (208 and 101 bp). L2-4 and L2-7 $T_0$ plants with two digested DNA bands (195 and 120 bp) were identified as positive mutants transformed with pVK005-SS2. For $T_0$ plants transformed with pVK005-SS3, L3-5 and L3-9 were called positive mutants, as the purified PCR product produced two digested DNA bands (184 and 165 bp; Fig. 1D). Genome-editing frequencies at sgRNA1 to sgRNA3 sites were 10.0%, 5.6%, and 15.4%, respectively (Table 1). This was the first time that the barley *SSIIa* gene was successfully mutagenised using RNA-guided Cas9, and a range of barley *ssIIa* allelic mutants were created. The mutation frequencies at these sites were equal to or slightly lower than those reported previously (Lawrenson et al., 2015).

### 3.2. Genetics of $T_0$ mutant plants

The nature of mutation of L1-2, L1-7, L2-4, L2-7, L3-5, and L3-9 mutant lines was analysed using Sanger sequencing after ligation of the PCR products and pEASY-T1 Vector. Varied mutation types of substitution, insertion or deletion involving single or more base pairs were found within target sites. Single base-pair insertion or substitution was more frequent than other mutation types in the transgenic lines. This study also found the deletion of multiple base pairs, such as a deletion of AGAC at the fourth base-pair upstream of the Protospacer Adjacent Motif (PAM) site in the line L1-2 generated from pVK005-SS1, a 15 bp TGCGGCGGTGTCCCT deletion at the second base-pair upstream of the PAM site, and a TTACG-to-C change at the region of the seed sequence in the transgenic line L2-4 (Fig. 1E). All mutations were typical indels induced by Cas9, which occurred at the 3 or 4 bp upstream of the PAM sequence (Cong et al., 2013). Most mutations resulted in a frameshift and the termination of *SSIIa* translation.

Non-destination mutation in genome-edited mutants is one of the drawbacks of CRISPR/Cas9 genome editing technology. In this study, genotypes were analysed at the potential off-target sites of L1-2, L1-7, L2-4, L2-7, L3-5, and L3-9. Based on the barley genomic data built into the web-based software (http://crispr.dbcls.jp), 0, 1, and 2 potential off-target sites were predicted for $T_0$ mutant plants transformed with pVK005-SS1 to pVK005-SS3, respectively. The results of sequencing showed that no mutation was found in these three predicted putative off-target sites (Supplementary Fig. 1). However, bioinformatic program can not retrieve all of the putative off-target sites in the barley genome completely, thus it is still possible off-target mutations happen in the

**Table 1**
Transformation efficiencies and mutation frequencies of *Agrobacterium*-mediated CRISPR/Cas9 targeted genome editing in barley.

| T-DNA construct | Embryo number | Regenerated lines | Surviving lines | Positive lines | Transformation efficiencies | Mutant plant | Mutation frequencies |
|---|---|---|---|---|---|---|---|
| *pVK005-SS1* | 110 | 20 | 20 | 20 | 18.2% | 2 | 10.0% |
| *pVK005-SS2* | 200 | 36 | 36 | 36 | 18.0% | 2 | 5.6% |
| *pVK005-SS3* | 60 | 13 | 13 | 13 | 21.7% | 2 | 15.4% |

Note: *pVK005-SS1* to *pVK005-SS3* representing three genome editing constructs containing sgRNA1 to sgRNA3, respectively.

whole barley genome. On the other hand, the $T_1$ homozygous mutants used for phenotypic analysis were identified from the offspring of three independent genome-edited lines L1-2, L2-7, and L3-9. They belong to three independent genetic backgrounds. All of them showed similar changes in grain morphology, grain composition, and starch properties. These findings excluded the adverse effects of off-target mutations on the reliability of the changes in the phenotype of *ssIIa* null mutants.

### 3.3. Identification and genetic analysis of ssIIa-null barley

Mature $T_1$ grains of $T_0$ mutant plants were harvested, and 266, 56, 225, and 68 grains were obtained from L1-2, L2-7, L3-5, and L3-9, respectively. No grains were produced from L1-7 and L2-4. Starch granule-associated proteins of all $T_1$ barley grains were analysed using SDS-PAGE, and 28, 4, and 4 homozygote *ssIIa*-null mutants were identified from $T_1$ progenies of L1-2, L2-7, and L3-9, respectively (Supplementary Table 2). For L3-5, no homozygous *SSIIa*-null offspring was obtained by self-crossing (Fig. 2). The results here differed from previous studies where genome-editing target sites were consistent with Mendelian genetics for a heterozygous mutation at a single locus (Li et al., 2021; Yang et al., 2020). More studies are needed to explain the unexpected genotyping results of *ssIIa* knocked out on grain development. $T_2$ grains were harvested from all $T_1$ homozygous *ssIIa*-null mutants. Ten $T_2$ grains of L1-2-1, L2-7-6, and L3-9-1 were randomly selected for analysing starch granule-associated proteins. For other $T_1$ *ssIIa*-null mutants, five $T_2$ grains of each plant were randomly chosen for SDS-PAGE analysis. The results indicated that all $T_2$ grains selected were *ssIIa*-null mutants on SDS-PAGE (Supplementary Fig. 2).

The genomic DNAs of those 28, 4, and 4 *ssIIa*-null progenies of L1-2, L2-7, and L3-9 were extracted at the second to third leaf stages. The sequence data from the corresponding sgRNA regions in these T1 mutants showed that the *ssIIa*-null mutant progenies of each mutant line had the same nucleotide mutations: an AGAC deletion in the L1-2 progenies, an A insertion in the L2-7 progenies, and a C insertion in the L3-9 progenies. Three $T_1$ progenies of L1-2, L2-7, and L3-9 and three $T_2$ mutant progenies of each selected $T_1$ mutant were randomly chosen for genotyping. Finally, the results showed that all $T_2$ progenies had identical genotypes as their corresponding $T_1$ plants, and as one type of the mutated nucleotides in the related $T_0$ plants (Supplementary Fig. 3). In addition, the results also confirmed the published conclusions that mutations in $T_1$ plants were transmitted to the $T_2$ generation without the occurrence of new mutations (Li et al., 2021; Yang et al., 2020).

Nontransgenic mutant progenies could be obtained by self-crossing of gene-edited mutants (Yang et al., 2020). In this study, $T_2$ grains of L1-2-1, L2-7-6, and L3-9-1 indicated by SDS-PAGE were germinated and transplanted in a greenhouse. The genomic DNAs of these $T_2$ plants were used as the PCR template to check for the absence or presence of the *Cas9* gene. The results showed that one, two, and three detected $T_2$ progenies of L1-2-1, L2-7-6, and L3-9-1 were Cas9-free plants, respectively (Supplementary Fig. 4A, C, and E). The hygromycin resistance tests showed that the leaf tips of $T_2$ plants without the *Cas9* gene turned yellow, as did the leaf tips from the Golden Promise control. The analyses above identified the T-DNA free plants from $T_2$ progenies of L1-2-1, L2-7-6, and L3-9-1 by both PCR detection and hygromycin resistance test (Supplementary Fig. 4B, D, and F).

The morphological data of $T_2$ mature grains were calculated and presented as the mean ± SD for each mutant line. All mutant grains showed a shrunken endosperm, with an apparent unfilled central region of the dorsal side of barley grains (Supplementary Fig. 5A). The TGW of mature grains in the mutant lines were significantly lower than that in NE lines (Supplementary Fig. 5B; Supplementary Table 3). Comparing the grain length, width, and area between mutant and NE grains showed only L2-7 grains had significantly reduced the grain width with 3.32 ± 0.06 mm compared to control lines with 3.55 ± 0.07 mm. All other parameters in mutant grains were not significantly different from NE grains (Supplementary Fig. 5B & D; Supplementary Table 4).

### 3.4. Mutated SSIIa proteins exhibit a loss of ADPG binding ability

The mutated SSIIa protein sequences of three genotypes of homozygous mutants were translated and aligned with the typical SSIIa protein sequence. The mutated SSIIa protein sequence of M292 and MK6827 were used as references (Morell et al., 2003). The initiation sites of the abnormal translation in different mutants were identified and marked (Fig. 3A; Supplementary Fig. 6). The results shown that although the premature stop codon induced by chemical mutagenesis in M292 and MK6827 appeared at different location to those induced by genome-editing in L1-2, L2-7, and L3-9, they all have destroyed the predicted function structures Pfam:Glyco_transf_5, Pfam:Glyco_transf_1, and Pfam:Glyco_transf_1_4. Although they lacked varied number of starch synthase active sites from two to three, the mutated SSIIa protein was not able to convert ADP-glucose into amylopectin. The loss of SSIIa function in these mutants affected the synthesis of amylopectin, leading to the change of the composition and structures of barley starch.

### 3.5. Mutation of ssIIa gene changed the activities of enzymes involved in starch biosythesis

The $T_2$ immature grains at 15 DAA of L1-2-1, L1-2-8, L1-2-47, L2-7-6, L2-7-7, L2-7-45, L3-9-1, L3-9-14, L3-9-47, and NE were used to assay the enzymatic activity of AGP, GBSS, SSS, SBE, and DBE. The results showed that the GBSS enzymatic activities of *ssIIa*-null mutant grains were significantly higher than that in NE. In contrast, the SSS and SBE enzymatic activities of *ssIIa*-null mutant grains were significantly lower than those in NE. For the AGP and DBE enzymatic activity, no apparent changes were detected in the grains between the *SSIIa*-null mutant and NE (Fig. 3B).

### 3.6. Loss of the SSIIa activity changed the genes expression of mutant barley grains

An early publication showed that the changes in the mRNA levels of SSI, SBEIIa and SBEIIb genes were not significant in barley ssIIa mutant compared to the controls. However, SBEIIb and SSI protein abundances were higher in the soluble stroma and inside starch granules of developing endosperm in barley ssIIa mutant than in control (Luo et al., 2015). For clarifying the expression discrepancies of the mRNAs and proteins between ssIIa mutant and control in barley, the RNA-seq analysis on *ssIIa* null mutants and NE at 15 DAA were performed to dissect the molecular basis of inactivation *SSIIa* gene on gene transcription in barley. Three comparison groups, L1-2 vs NE, L2-7 vs NE, and L3-9 vs NE produced 1209, 1090, and 1406 differentially expressed genes (DEGs), respectively. The Gene Ontology (GO) analysis of the DEGs indicated that multiple cellular component, molecular function,

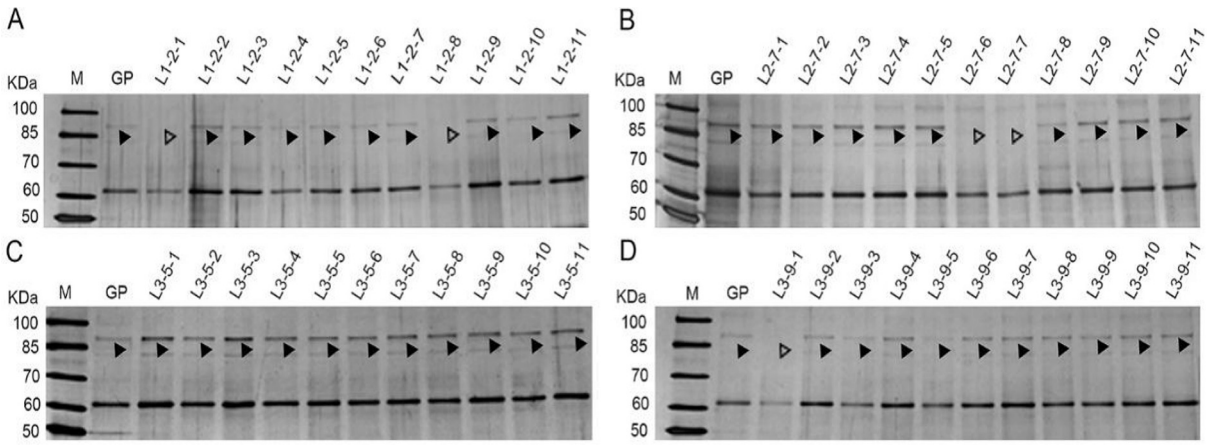


**Fig. 2.** SDS-PAGE analysis of $T_1$ mutant grains of barley *ssIIa* mutants.
(A) $T_1$ grains of L1-2. (B) $T_1$ grains of L2-7. (C) $T_1$ grains of L3-5. (D) $T_1$ grains of L3-9. M, protein ladder (the size of each band is labelled at the left side of SDS-PAGE gels); GP, Golden Promise, nontransgenic donor barley (Lx-x-x represents the grains of different mutant lines, e.g., L1-2-1 represents the number 1 grain of L1-2 line). Arrows indicate expressed SSIIa protein (solid) or the absence of *SSIIa* protein (hollow).

and biological process were affected by the *SSIIa* gene knockout in barley. These included many metabolic and biosynthetic processes, and the starch metabolic process, glucan metabolic process, beta-glucan biosynthetic process etc. were selected to shown in detail (Supplementary Fig. 7).

The RNA-seq data of genes related to barley starch biosynthesis showed that *HvGBSSI*, and *HvSSI* were higher than that of the NE while the transcript levels of the *HvSSIIa*, *HvSBEI*, and *HvPUL* were lower than that of the NE (Fig. 4A). For the transcript levels of the *HvAGPS*, *HvAGPL*, *HvSSIIIa*, *HvSSIIIb*, *HvSSIVa*, *HvSBEIIa*, *HvSBEIIb*, *HvISAI*, *HvISAII*, and *HvISAIII*, no obviouse changes were detected between the *SSIIa*-null mutant and NE. To verify the reliability of RNA-seq data, starch biosynthetic genes were chosen to validate by qRT-PCR. The results of qRT-PCR were consistent with the RNA-seq data (Fig. 4B; Supplementary Fig. 8), indicated that the transcriptome data of RNA-seq is reliable. The increased expression of *HvGBSSI* explained the increase of GBSS enzymatic activity, the decreased expression of *HvSSIIa* and *HvSBEI* were responsible for the decrease of SSS and SBE enzymatic activity, respectively. According to the results of enzymatic activity, the increased expression of *HvSSI* cannot effectively compensate for the loss of *HvSSIIa*.

### 3.7. Metabolic pathway in the endosperm of ssIIa null barley

A metabolic pathway in the endosperm of barley was constructed and shown in Fig. 5. The pathway includes the biosynthesis of amino acids, glycolysis and starch biosynthesis, tricarboxylic acid cycle (TCA), energy-related metabolism, and lipid metabolism. Some of the genes and metabolites involved in this pathway were listed in Supplementary Fig 9. The relative expressional levels of these genes and the accumulation of metabolites in *ssIIa* null mutants were calculated and shown in Supplementary Tables 5 & 6, respectively. In the process of glycolysis and starch biosynthesis, the expression of metabolites G6P, F6P, ADP-glucose, and the *PGM* gene in the mutants increased obviously. These results suggested that the processes of glycolysis and starch biosynthesis were activated in the mutants. However, the expression of 3PG in the mutant showed no increase compared to that in NE. The activation of the subsequent steps for glycolysis maybe limited by the slight decreasing or ineffective increasing of 6-phosphofructo-1-kinase (PFK). Previous study indicated our inference that metabolic flux through the glycolytic pathway was tightly regulated, and the most complex control was exerted on PFK level (Aleksandra & Matic, 2010). For the starch biosynthesis process, typically, the increased ADP-glucose can activate the subsequent pathway of starch biosynthesis. However, there were no obvious changes for AGP enzymatic activity in the mutant. It was well known that the reaction from ADP-glucose to active ADPG was catalysed by AGP enzymes (Bowsher et al., 2007). The unchanged AGP enzymatic activity was consistent with the shrunken grains of ssIIa mutant, as mutant grains having significantly lower 1000 seed weight than that in the NE. In the TCA cycle, some of the genes involved in the process such as *CS*, *IDH*, *OGDH*, *DLST*, *LSC1*, *FUM*, and *MDH* in the mutants, showed a higher expression compared to that in NE. However, most of the metabolites in TCA cycle process were not increase. The inconsistent trend of changes in the genes and metabolites in TCA cycle indicate that the inactivation of the *SSIIa* gene has an activation effect on TCA cycle. However, due to the limited sythesis of the upstream metabolite like 3PG, the accumulation of metabolites involved in TCA cycle cannot increase effectively. For other metabolites such as Asparagine, LysoPC, Lysine, and Histidine, the changes in the accumulation were all limited by upstream metabolites.

In summary, the inactivation of *SSIIa* gene activated part of glycolysis and starch biosynthesis pathway. The PFK and AGP enzymatic activity limited the activation of other processes directly or indirectly. There were not enough metabolite increases that could compensate for the decrease in starch biosynthesis. This can explain the reduction of barley 1000-grain weight in the perspective of metabolite accumulation.

### 3.8. Starch compositions and digestion properties of mutant barley grains

The contents of total starch, amylose, RS, and starch digestion properties of mature grains of mutant lines and NE lines were measured. $T_2$ grains of L1-2-1, L1-2-8, L1-2-47, L2-7-6, L2-7-7, L2-7-45, L3-9-1, L3-9-14, and L3-9-47 were randomly selected to measure the starch composition of three mutant lines L1-2, L2-7, and L3-9. The composition of $T_2$ grains indicated that the total starch contents of mutant lines L1-2, L2-7, and L3-9 was significantly lower than NE grains. The AC (Amylose Assay Kit) of mutant lines L1-2 (43.23% ± 5.05%, mean ± SD), L3-7 (51.56% ± 3.84%), and L4-9 (51.67% ± 0.52%) were about two fold of that in NE lines (24.38% ± 0.96%). Moreover, the RS (RS1) contents in mutant lines L1-2, L2-7, and L3-9 were 2.41% ± 0.15%, 2.45% ± 0.13%, and 2.86% ± 0.07%, respectively, which were more than sixfold of that in NE lines (0.35% ± 0.02%; Fig. 6A; Supplementary Table 7). In summary, the changes in starch composition were consistent with the typical characteristics of high-amylose barley and wheat, with significantly increased AC and RS (Li et al., 2011; Li et al., 2021; Morell et al., 2003; Regina et al., 2006).

The digestion properties of mutant barley grain were analysed by in vitro digestibility. The results of the proportion of RDS, SDS, and RS

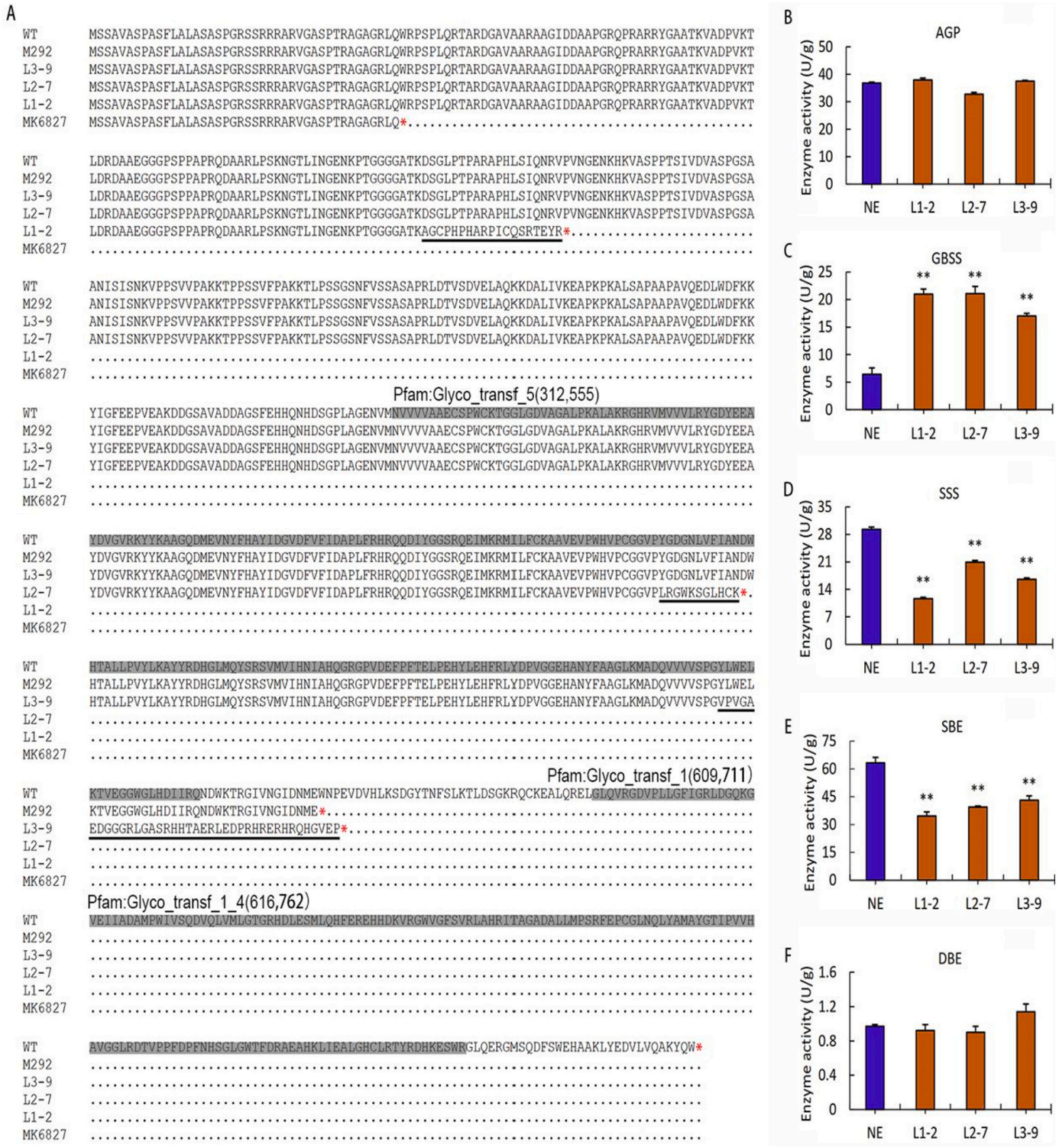


**Fig. 3.** The missing starch synthase active sites and expression levels of starch synthetic enzymatic activities of barley *ssIIa* mutants.
(A) The genome-edited induced mutations and the chemical-induced mutations affect different starch synthase active sites. WT, the SSIIa protein sequence of Golden Promise; L1-2, L2-7, and L3-9, the SSIIa protein sequences of genome-edited lines L1-2, L2-7, and L3-9, respectively; M292 and MK6827, the SSIIa protein sequences of chemical induced mutants published by Morell et al.; the asterisks represent the termination codons; the sequences in black boxes represent the protein structure domains, Pfam:Glyco_transf_5, Pfam:Glyco_transf_1, and Pfam:Glyco_transf_1_4; the underlined sequences indicate the incorrectly translated protein sequences. (B–F) The enzymatic activities of AGP, GBSS, SSS, SBE, and DBE of barley ssIIa null mutants and NE lines. The asterisks indicate the statistical significance between the non-genome edited grains (NE) and the mutant grains determined by Student's *t*-tests (* at $P < 0.05$; ** at $P < 0.01$).

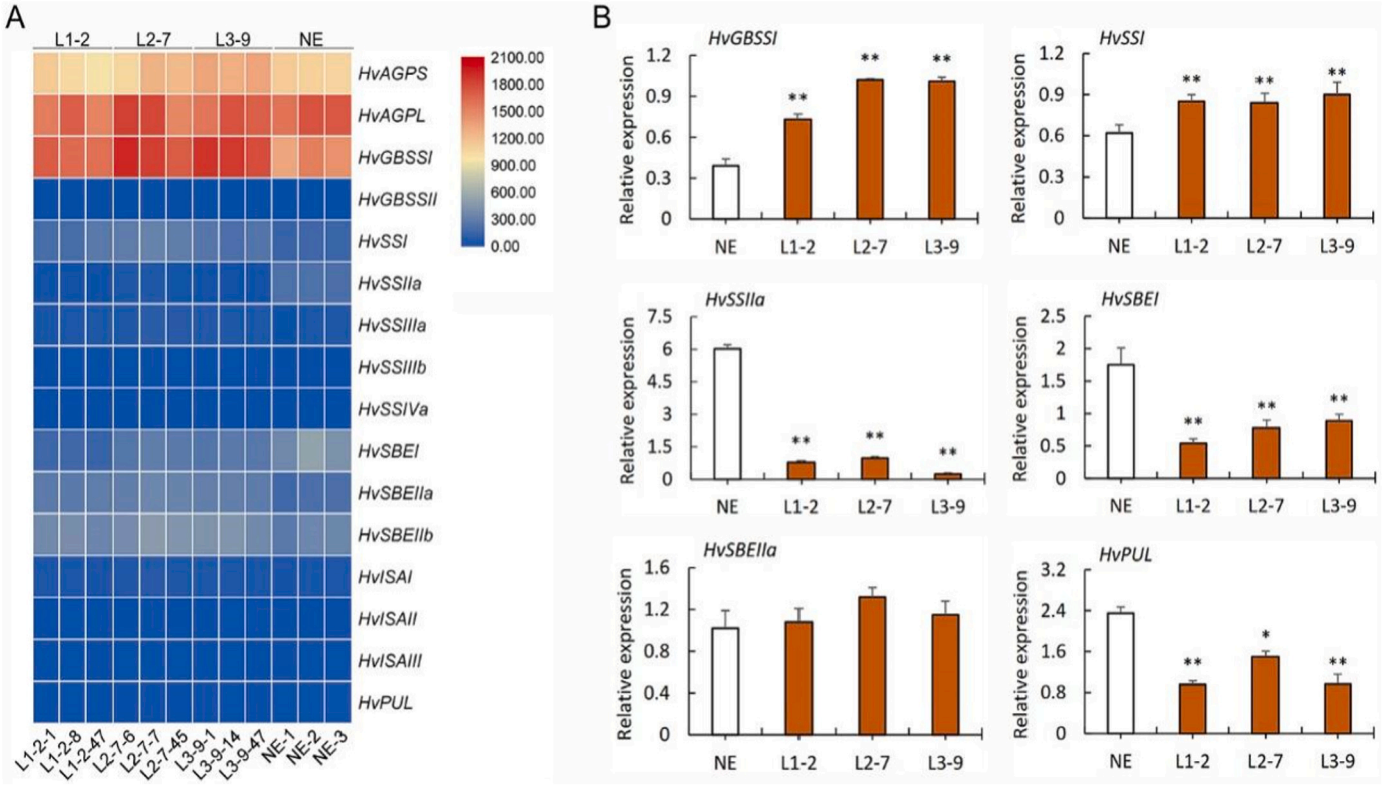


**Fig. 4.** Starch biosynthesis-related genes are regulated by the barley *SSIIa* gene.
(A) Heat map of starch biosynthesis-related genes in *SSIIa* null mutants and NE. (B) qRT-PCR analysis of *HvGBSSI*, *HvSSI*, *HvSSIIa*, *HvSBEI*, *HvSBEIIa*, and *HvPUL* expression in the *SSIIa* null mutants. Asterisks indicate the statistical significance between the non-genome edited grains and the mutant grains determined by Student's *t*-tests (* at $P < 0.05$; ** at $P < 0.01$).

(calculated by different formulas from the standard kit, designated as RS2) of grain starch were calculated in the mutant and NE barley. The proportion of RDS, SDS, and RS2 in all mutant lines L1-2, L2-7, and L3-9 varied from 22.80% ± 3.08% to 33.67% ± 1.59%, from 8.69% ± 1.08% to 14.19% ± 1.70%, and from 52.68% ± 1.84% to 62.50% ± 2.22% respectively, which were significantly different from the corresponding parameter of NE lines, with the proportion of RDS, SDS, and RS2 at 45.04% ± 0.14%, 21.07% ± 0.66%, and 30.70% ± 1.47%, respectively. The results indicated that the knockout *SSIIa* gene in barley induced a significant decrease of RDS and SDS compared to a substantial increase of RS2 in approximately two folds (Fig. 6B; Supplementary Table 8). Comparison of RS1 and RS2 in the *ssIIa* mutant grains showed that the values of RS2 were about 20 folds of that in RS1. However, RS1 had more increased folds than RS2 compared with their non-genome-edited lines, respectively. Therefore, it is crucial to check the methods and materials (e.g. wholemeal or starch) used when comparing RS contents among the published data. The increase in both the RS1 and RS2 indicated that the deletion of the *SSIIa* gene could significantly improve the digestibility of barley starch.

Due to the nutritional benefits and health effects of the composition of barley grains, there is a growing demand for barley as an ingredient in food production. Based on the requirements of the diet for improved public health, modification of the starch composition of barley grains to increase the amylose/RS content can enhance its value in food production (Baik & Ullrich, 2008). However, due to the low amylose and RS content in barley cultivars, it isn't easy to improve the RS content of barley by traditional breeding methods (Zhu, 2017). The barley *ssIIa* null mutants Himaraya292 (BARLEYmax) were generated by chemical mutagenesis, possesses elvated amylose contents of about 60%, which further led to the significantly increase of RS and other bioactive ingredients compared to wild type line (Morell et al., 2003). Studies in rats and pigs indicated that consumption of *ssIIa* null barley can reduce the plasma cholesterol, modify the microbiota, alter the large bowel SCFA and PH value consequently (Aoe et al., 2019; Bird, Flory, et al., 2004; Bird, Jackson, et al., 2004). In this study, we generated barley mutants by the targeted mutagenesis of the *SSIIa* gene using RNA-guided Cas9, these edited mutants also has high amylose contents of ~50%, and greatly increased RS, plus irregular starch granule shapes, these were similar to those of Himaraya292, indicating genome edited *ssIIa* null barley mutants are valuable for health. Thus, this work producing homozygous mutants with altered starch composition and digestion properties using targeted editing, provided a fast approach to deliver the potential benefits for improving human health.

### 3.9. Starch structure in ssIIa-null mutants

Starch from genome edited lines and NE lines was used to analyse the starch properties of *ssIIa*-null mutants. Data from L1-2, L2-7, and L3-9 represented the average values of three tested offspring of the corresponding mutant lines.

The chain length distribution of debranched starch was analysed using FACE, and the normalised chain length distribution of mutant lines and NE are shown in Fig. 6C. The differences of the normalised chain length distribution between each mutant and NE lines were calculated by subtracting the data of NE from the data of the corresponding mutant line (Fig. 6D). Based on the differences between mutants and NE, the percentages of chain lengths were divided in four groups, DP6-12, DP13-28, DP29-34, and DP35-70, in which the total values of DP6-70 were defined as 100%. The results showed that the targeted inactivation of the *SSIIa* gene significantly increased the proportion of shorter chains with DP6-12, decreased the proportion with DP13-28, increased the proportion with DP29-34, and decreased the proportion with DP35-70 compared to that in the NE control (Table 2).

The thermal characteristics of mutant barley starches was measured

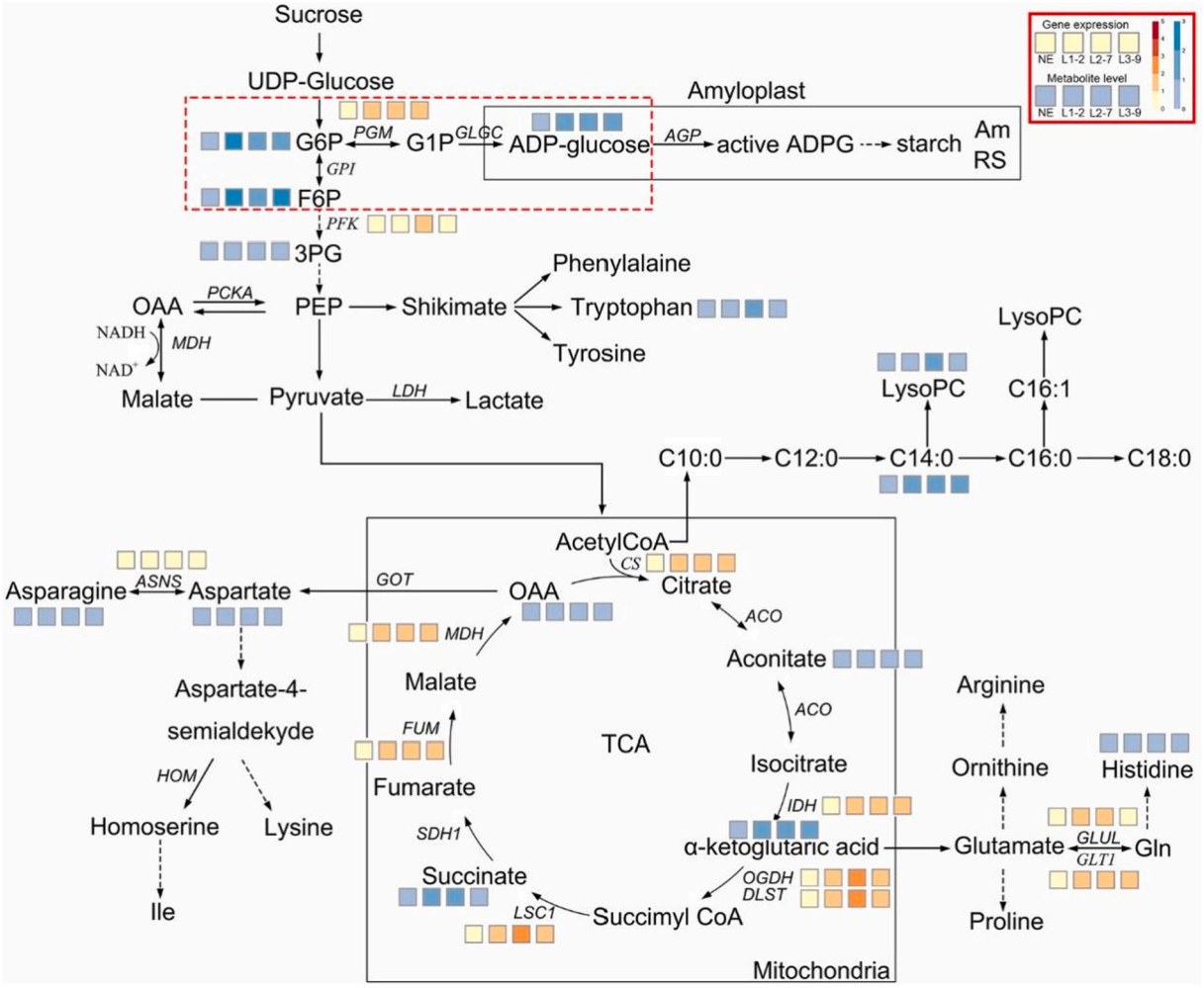


**Fig. 5.** Metabolic pathway in the endosperm of *ssIIa* null barley.
The changes of metabolite and gene expression in barley endosperm are shown as heat maps. The heat maps for the expression levels of gene and metabolite are in blue and yellow boxes, respectively. The expressional levels of each gene and metabolite in NE are defined as 1. The solid arrows indicate that there are no intermediated steps between the two metabolites, and the dotted arrows indicate that some intermediate metabolites are omitted in the pathway between the two metabolites. (For interpretation of the references to colour in this figure legend, the reader is referred to the web version of this article.)

using DSC. The onset (To), peak (Tp), and final or completed (Tc) gelatinisation temperature and gelatinisation enthalpy (ΔH values) of mutant lines L1-2, L2-7, and L3-9 were significantly lower than the corresponding parameter of NE (Fig. 6F). Previous studies using this method demonstrated that starch with high AC has a higher gelatinisation temperature (Fuwa et al., 1999; Krueger et al., 1987). However, in this study, the gelatinisation temperature of high AC mutants L1-2, L2-7, and L3-9 was lower than NE (Fig. 6F).

Combining the results of DSC and FACE, the counterintuitive data of DSC can be explained by the fact that knockout of the *SSIIa* gene altered the chain length distribution of barley starch (Table 2), by significantly increasing the proportion of short branch chains (DP6-12), further led to the average amylopectin branch chain lengths of *ssIIa*-null starch were shorter than NE barley starch. Thus, the starch from *ssIIa*-null mutants has a shorter average amylopectin branch chain length and lower gelatinisation temperatures than NE. Previous work indicated that amylose contents and amylopectin branch chain length distributions play a key role in determination of the pasting properties of starch. The similar case was also found in starches with large proportions of short branch chains, or with short average amylopectin chain lengths, or with high content of starch phosphate monoester displayed low gelatinisation temperatures (Jane et al., 1999).

The molecular weight distribution of debranched barley starch was analysed by SEC, the contents of amylose (Am) and amylopectin (Ap) of barley starch from each mutant line were calculated according to the SEC data (Fig. 6E). The Am of mutant lines was about double that of NE. Moreover, the Ap contents in mutant lines was significantly reduced compared to the content in NE. The Am/Ap ratios in L1-2, L2-7, and L3-9 was 1.64 ± 0.19, 1.61 ± 0.11, and 1.57 ± 0.27, respectively, significantly higher than 0.48 ± 0.00 in NE (Table 2). Am contents of mutant grains from SEC assay were approximately 10% higher than those from the Amylose Assay Kit (Megazymme), but both SEC and Amylose Assay Kit gave similar ratios between mutants and NE.

The crystalline structure of mutant barley starches was analysed using $^{13}C$ solid-state NMR. The signals at 59 to 62, 81 to 84, and 99 to 104 ppm were assigned to hydroxymethyl carbon 6 (C6), C4, and C1, respectively, and the signal at 70 to 73 ppm was associated with C2,3,5 in hexopyranoses (Cheetham & Tao, 1998). In present study, the high-resolution resonances of $^{13}C$ NMR spectra were different between the starches of *ssIIa*-null and NE barley. Four C1 peaks were detected in the NE barley starch sample as normal cereal starch, but only one C1 peak was detected in L1-2, L2-7, and L3-9. Two C6 peaks were detected in L1-2, L2-7, and L3-9 compared to only one C6 peak in the NE sample (Fig. 6G). The resonance intensities at C1, C2,3,5, and C4 of the *ssIIa*-null sample were higher than that in the corresponding NE sample, and the resonance intensity of the C6 peak in the NE sample was higher than the

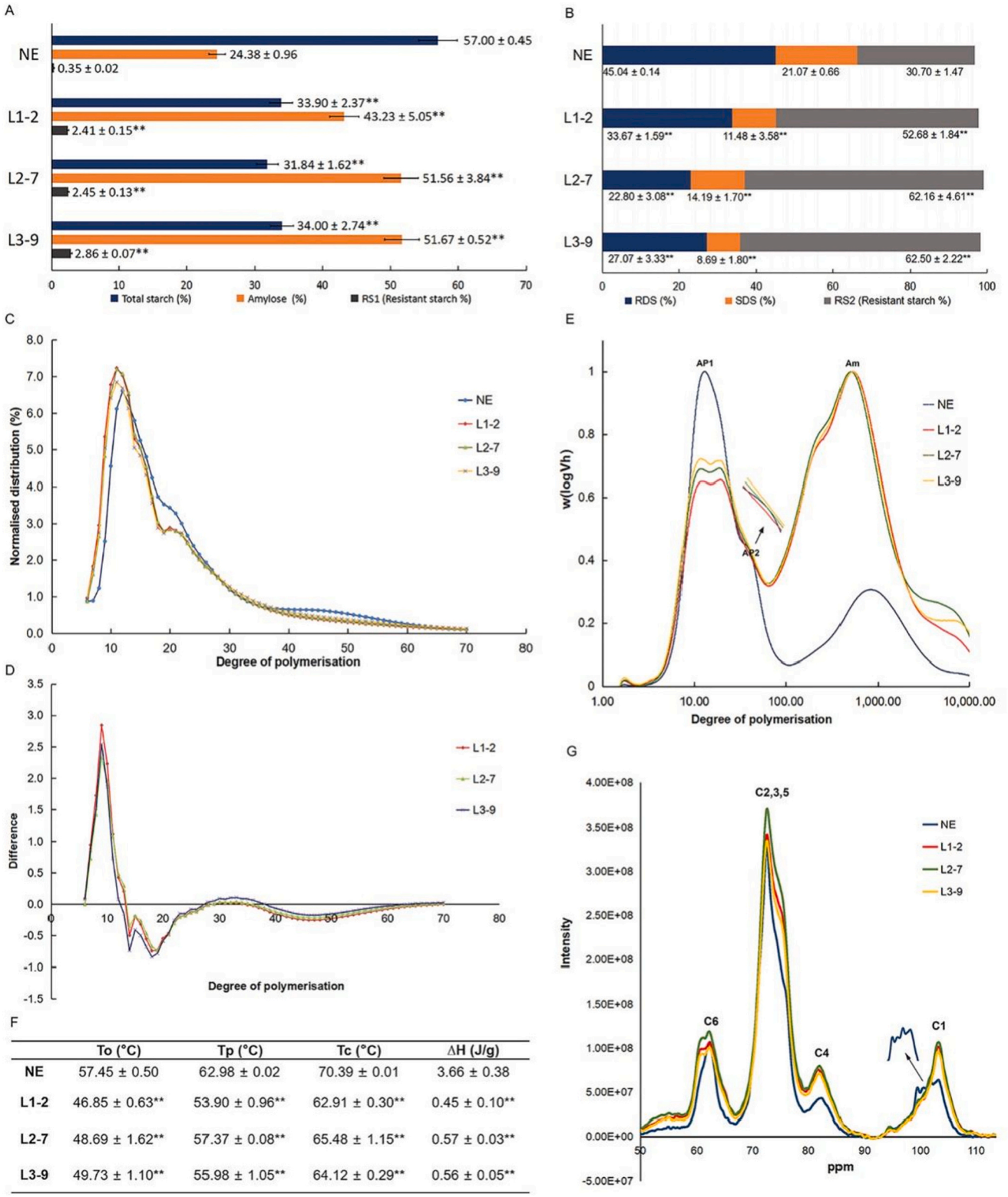


F

| | To (°C) | Tp (°C) | Tc (°C) | ΔH (J/g) |
|---|---|---|---|---|
| NE | 57.45 ± 0.50 | 62.98 ± 0.02 | 70.39 ± 0.01 | 3.66 ± 0.38 |
| L1-2 | 46.85 ± 0.63** | 53.90 ± 0.96** | 62.91 ± 0.30** | 0.45 ± 0.10** |
| L2-7 | 48.69 ± 1.62** | 57.37 ± 0.08** | 65.48 ± 1.15** | 0.57 ± 0.03** |
| L3-9 | 49.73 ± 1.10** | 55.98 ± 1.05** | 64.12 ± 0.29** | 0.56 ± 0.05** |

**Fig. 6.** Composition and starch properties of $T_2$ mutant grains of barley *ssIIa* mutants.
(A) Constituents of total starch, apparent amylose, and RS. RS1, RS content measured by the Megazyme RS Assay Kit. (B) Constituents of RDS, SDS, and RS in the starch of mutant barley grains. RDS, average RDS content; SDS, average SDS content; RS2, average RS content calculated by a formula published by Englyst et al. (C) Normalised chain length distribution. (D) Differences in chain length distributions between mutants and NE. The names of the $T_1$ mutant lines and NE are labelled on the right side. (E) SEC molecular weight distributions of debranched barley starch. AP1, amylopectin peak; AP2, long-chain amylopectin peak; Am, amylose peak. The names of the $T_1$ mutant lines and NE are labelled on the right side. (F) Gelatinisation temperature measured by DSC. The onset (To), peak (Tp), and final or completed (Tc) gelatinisation temperature and gelatinisation enthalpy (ΔH) were calculated. The names of the $T_1$ mutant lines and NE are labelled on the left side. (G) Solid-state NMR spectra of *ssIIa* null and NE starches. C1, C2,3,5, C4, and C6 represent the corresponding hydroxymethyl carbon signal peaks. Data of NE, L1-2, L2-7, and L3-9 are the mean of three biological replicates for the corresponding parameters. Asterisks indicate the statistical significance between the non-genome edited grains and the mutant grains determined by Student's *t*-tests (* at $P < 0.05$; ** at $P < 0.01$).

**Table 2**
Chain length distribution and starch composition of debranched barley starch.

| Line | DP (%) (FACE) | | | | Starch composition (SEC) | | |
|---|---|---|---|---|---|---|---|
| | DP6–12 | DP13–28 | DP29–34 | DP35–70 | Am (%) | Ap (%) | Am/Ap |
| NE | 22.75 ± 4.10 | 55.69 ± 3.30 | 6.24 ± 0.48 | 15.32 ± 0.32 | 32.16 ± 0.20 | 67.84 ± 0.20 | 0.48 ± 0.00 |
| L1-2 | 32.10 ± 0.44** | 50.83 ± 0.98** | 6.30 ± 0.12 | 10.76 ± 0.93** | 61.95 ± 2.71** | 38.05 ± 2.71** | 1.64 ± 0.19** |
| L2-7 | 30.72 ± 2.60** | 51.17 ± 1.51** | 6.38 ± 0.25 | 11.73 ± 1.17** | 61.64 ± 1.64** | 38.36 ± 1.64** | 1.61 ± 0.11** |
| L3-9 | 30.41 ± 0.92** | 49.79 ± 0.93** | 6.74 ± 0.34* | 13.06 ± 1.45* | 60.72 ± 4.06** | 39.28 ± 4.06** | 1.57 ± 0.27** |

Mean ± SD from duplicates of three progenies of the corresponding mutation line.
* $0.01 < P < 0.05$, significant difference between mutant and WT.
** $P < 0.01$, highly significant difference between mutant and WT.

second C6 peak of L2-7 and L3-9 but weaker than L1-2 (Fig. 6G; Table 3). The inactivation of the *SSIIa* gene altered the peak numbers in C1 and C6 peaks, and the resonance intensities at each peak. Previous studies indicated that starches with different amylose content have similar 13C NMR spectra in the solid state (Cheetham & Tao, 1998), the peak numbers in C1 peak is a character for different type of starch (Li et al., 2020). We found that the starch from NE was identified as A-type starch which contain four C1 peaks with a weak peak included, while the *ssIIa* null mutant starch was observed to have a single C1 peak (Fig. 6G). The results showed that the starch from NE and *ssIIa* null mutants belonged to different crystalline structure. Wei et al. mentioned that the C1 peak at 102.9 ppm (~103 ppm in the present study) corresponds to the content of amylose-lipid complex in starch (Wei et al., 2010). Our results showed that the resonance intensities of the C1 peak at ~103 ppm in the mutant was significantly higher than that in NE. This indicated that starch from *ssIIa* null mutant contained a higher content of the amylose-lipid complex (ALCs) (Li et al., 2020). According to the conclusions of previous studies, ALCs are classified as resistant starch types III or V, the regular consumption of foods containing ALCs has been shown to reduce blood glucose levels in humans (Panyoo & Emmambux, 2017). A transgenic rice line enriched amylose and RS contained a higher amylose-lipid complex has been shown to have higher digestibility than controls (Wei et al., 2010). All of the conclusions above indicated that the inaction of the *SSIIa* gene changed the crystalline structure, increased the content of ALCs, resulting in higher digestibility of barley starch.

### 3.10. Starch granule morphology

The starch granules of L1-2-1, L2-7-6, and L3-9-1 were used to analyse the microstructure of mutant grains. The starch granules of Golden Promise and NE were used as control. Both the SEM and iodine staining results showed apparent differences in the microstructure of starch granule between mutants and controls. The morphology of A-type starch granules in mutant grains was altered, with an apparent hollow surface but was normally spherical in Golden Promise and NE (Fig. 7A–D). The analyses of the percentage of A- and B-type starch granule in the mutants and control showed that the number percentages of A-type starch granules in mutants were higher than that in the control. However, the volume percentages of A-type starch in mutants were lower than that in the control. The results is reflected that the volumes of A-type starch granules in the mutants were smaller than typical granules in the control (Supplementary Table 9). The results confirmed the observations from early study (Morell et al., 2003).

### 3.11. Improving the health benefits of barley with SSIIa knockout

Indels were induced by genome editing, resulting in frameshift mutations and leading to the prematurely terminated translation of the *SSIIa* gene (Supplementary Fig. 6). The enzymatic activity of the *ssIIa* null mutant had obvious changes. The SSS enzymatic activity was significantly decreased, while the GBSS enzymic activity was substantially higher than that in NE (Fig. 3B). The average amylopectin branch chain lengths of *ssIIa*-null starch were decreased and the crystalline structure changed with the content of amylose-lipid complex increased. In addition, the contents of amylose and RS in the mutant were significantly higher than that in NE (Fig. 6A). The higher content of amylose-lipid complex and RS significantly improved the digestibility of starch from mutant barley. This conclusion demonstrated the health benefits of starch from mutant barley.

## 4. Conclusions

In this study, a range of barley *ssIIa* null mutants were created by the genome editing approach. The destruction of ADPG binding structure has led to the inactivation of SSIIa in edited lines. The amylose and RS contents in mutant grains increased dramatically, about two- and sixfold that of NE. The starch of mutant grains had higher resistance to starch digestion than NE. For the starch properties, the reduction of the average intermediate amylopectin branch chain lengths in mutant lines resulted in an abnormal thermal characterisation with a high AC starch having low To, Tp, Tc, and ΔH values in mutants compared to NE. The changed crystalline structure in the mutant starch resulted in different $^{13}C$ NMR spectra and high resonance intensities at the peak corresponding to the amylose-lipid complex, which may link with the mutant starch having a slow digestibility. The RNA-seq and qRT-PCR analyses showed that the barley *ssIIa* mutant had significantly increased expressions of *HvGBSSI* and *HvSSI*, and reduced expressions of *HvSSIIa*, *HvSBEI*, and *HvPUL*. Such changed transcript expressions led to the changes in starch content, starch structure and properties. The metabolic pathway in the endosperm showed that no increase in metabolite production could compensate for the decrease of starch, which explained the reduction of barley grain weight. Our work further understood the changes in starch and grain properties of healthy grains of *ssIIa* mutant barley, which is widely used for humans' healthy diet. However, the phenotype of the shrunken endosperm in the mutants decreases the yield, limiting its

**Table 3**
$^{13}C$ NMR chemical shifts of barley starch.

| Line | Chemical Shifts ($^{13}C$ NMR) | | | | | | | |
|---|---|---|---|---|---|---|---|---|
| | C1 ppm (intensity) | | | | C4 ppm (intensity) | C2,3,5 ppm (intensity) | C6 ppm (intensity) | |
| NE ($1 \times 10^7$) | 99.50 (5.49) | 100.57 (5.48) | 101.73 (6.55) | 103.21 (6.37) | 82.37 (4.31) | 72.57 (32.69) | – | 62.36 (10.68) |
| L1-2 ($1 \times 10^7$) | – | – | – | 103.26 (10.65) | 82.00 (7.94) | 72.67 (37.01) | 61.11 (11.16) | 62.22 (11.87) |
| L2-7 ($1 \times 10^7$) | – | – | – | 103.26 (10.15) | 81.81 (7.54) | 72.62 (34.17) | 60.87 (9.88) | 62.31 (10.61) |
| L3-9 ($1 \times 10^7$) | – | – | – | 103.17 (9.58) | 82.04 (7.09) | 72.62 (33.43) | 60.97 (9.32) | 62.27 (10.01) |

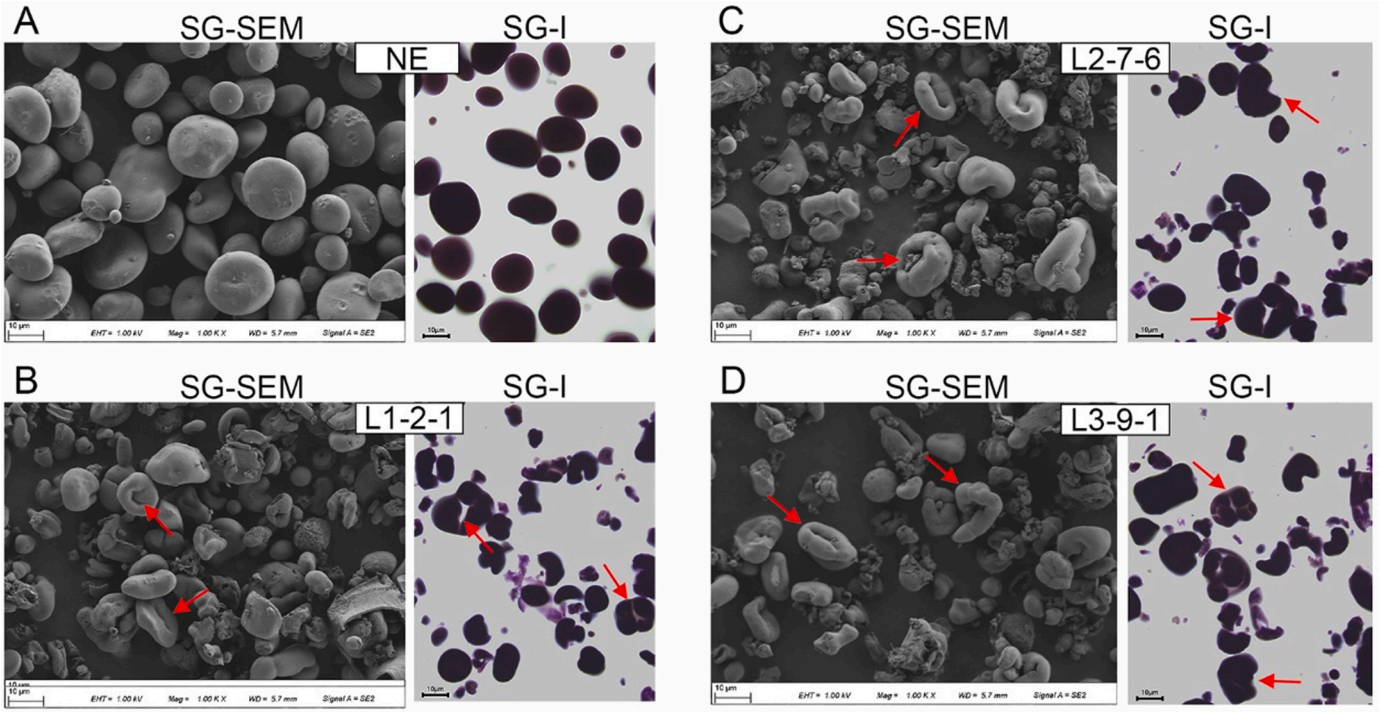


**Fig. 7.** Scanning electron micrographs and iodine staining of purified starch granules.
(A) Non-genome-edited line. (B) L1-2-1. (C) L2-7-6. (D) L3-9-1. SG-SEM represent the SEM images of purified starch granules. SG-I represent the iodine staining images of purified starch granules. The red arrow indicates a deformed starch granule in the mutants.

applications.

Supplementary data to this article can be found online at https://doi.org/10.1016/j.carbpol.2022.119238.

## CRediT authorship contribution statement

**Qiang Yang:** Validation, Formal analysis, Data curation, Investigation, Writing – original draft. **Jinjin Ding:** Formal analysis, Methodology, Resources, Visualization. **Xiuqin Feng:** Formal analysis, Methodology, Resources, Visualization. **Xiaojuan Zhong:** Formal analysis, Methodology, Resources, Visualization. **Jingyu Lan:** Formal analysis, Methodology, Resources, Visualization. **Huaping Tang:** Formal analysis, Methodology, Resources, Visualization. **Wendy Harwood:** Methodology, Software, Writing – review & editing. **Zhongyi Li:** Methodology, Software, Writing – review & editing. **Carlos Guzmán:** Methodology, Software, Writing – review & editing. **Qiang Xu:** Methodology, Visualization, Writing – review & editing. **Yazhou Zhang:** Methodology, Visualization, Writing – review & editing. **Yunfeng Jiang:** Methodology, Visualization, Writing – review & editing. **Pengfei Qi:** Methodology, Visualization, Writing – review & editing. **Mei Deng:** Methodology, Visualization, Writing – review & editing. **Jian Ma:** Writing – review & editing. **Jirui Wang:** Writing – review & editing. **Guoyue Chen:** Writing – review & editing. **Xiujin Lan:** Writing – review & editing. **Yuming Wei:** Supervision, Funding acquisition. **Youliang Zheng:** Supervision, Funding acquisition. **Qiantao Jiang:** Conceptualization, Supervision, Funding acquisition, Project administration, Writing – review & editing.

## Declaration of competing interest

The authors declare that they have no known competing financial interests or personal relationships that could have appeared to influence the work reported in this paper.

## Acknowledgments

This work was supported by the Sichuan Science and Technology Program, China (2021YFH0111), and the International Science & Technology Cooperation Project of Chengdu, Sichuan Province, China (2019-GH02-00078-HZ). Carlos Guzmán acknowledges the European Social Fund and the Spanish State Research Agency (Ministry of Science, Innovation and Universities) for the funding through the Ramon y Cajal Program (RYC-2017-21891).

## References

Aleksandra, U., & Matic, L. (2010). Evolution of allosteric citrate binding sites on 6-phosphofructo-1-kinase. *PLoS One, 5*(11). https://doi.org/10.1371/journal.pone.0015447

Aoe, S., Yamanaka, C., Fuwa, M., Tamiya, T., Nakayama, Y., Miyoshi, T., & Kitazono, E. (2019). Effects of BARLEYmax and high-β-glucan barley line on short-chain fatty acids production and microbiota from the cecum to the distal colon in rats. *PLoS One, 14*(6). https://doi.org/10.1371/journal.pone.0218118

Baik, B. K., & Ullrich, S. E. (2008). Barley for food: Characteristics, improvement, and renewed interest. *Journal of Cereal Science, 48*(2), 233–242. https://doi.org/10.1016/j.jcs.2008.02.002

Bekesiova, I., Nap, J. P., & Mlynarova, L. (1999). Isolation of high quality DNA and RNA from leaves of the carnivorous plant *Drosera rotundifolia*. *Plant Molecular Biology Reporter, 17*(3), 269–277. https://doi.org/10.1023/A:1007627509824

Bird, A. R., Brown, I. L., & Topping, D. L. (2000). Starches, resistant starches, the gut microflora and human health. *Current Issues in Intestinal Microbiology, 1*(1), 25–37. https://doi.org/10.1016/S0140-6736(01)34809-2

Bird, A. R., Flory, C., Davies, D. A., Usher, S., & Topping, D. L. (2004). A novel barley cultivar (Himalaya 292) with a specific gene mutation in starch synthase IIa raises large bowel starch and short-chain fatty acids in rats. *The Journal of Nutrition, 134*(4), 831–835. https://doi.org/10.1093/jn/134.4.831

Bird, A. R., Jackson, M., King, R. A., Davies, D. A., Usher, S., & Topping, D. L. (2004). A novel high-amylose barley cultivar (*Hordeum vulgare* var. Himalaya 292) lowers plasma cholesterol and alters indices of large-bowel fermentation in pigs. *British Journal of Nutrition, 92*(4), 607–615. https://doi.org/10.1079/BJN20041248

Bowsher, C. G., Scrase-Field, E. F. A. L., Esposito, S., Emes, M. J., & Tetlow, I. J. (2007). Characterization of ADP-glucose transport across the cereal endosperm amyloplast envelope. *Journal of Experimental Botany, 58*(6), 1321–1332. https://doi.org/10.1093/jxb/erl297

Briggs, D. E. (2012). *Barley*. New York: Springer Science & Business Media.

Cave, R. A., Seabrook, S. A., Gidley, M. J., & Gilbert, R. G. (2009). Characterization of starch by size-exclusion chromatography: The limitations imposed by shear scission. *Biomacromolecules, 10*(8), 2245–2253. https://doi.org/10.1021/bm900426n

Cheetham, N. W., & Tao, L. (1998). Solid state NMR studies on the structural and conformational properties of natural maize starches. *Carbohydrate Polymers, 36*(4), 285–292. https://doi.org/10.1016/S0144-8617(98)00004-6

Cong, L., Ran, F., Cox, D., Lin, S., Barretto, R., Habib, N., … Zhang, F. J. S. (2013). Multiplex genome engineering using CRISPR/Cas systems. *339*(6121), 819–823. https://doi.org/10.1126/science.1231143

Englyst, H. N., Kingman, S. M., & Cummings, J. (1992). Classification and measurement of nutritionally important starch fractions. *European Journal of Clinical Nutrition, 46*, S33–S50.

Fan, X. Y., Guo, M., Li, R. D., Yang, Y. H., Liu, M., Zhu, Q., Tang, S. Z., Gu, M. H., Xu, R. G., & Yan, C. J. (2017). Allelic variations in the soluble starch synthase II gene family result in changes of grain quality and starch properties in rice (*Oryza sativa* L.). *The Journal of Agricultural Science, 155*(1), 129–140. https://doi.org/10.1017/S0021859615001331

Fan, X. Y., Zhu, J., Dong, W. B., Sun, Y. D., Lv, C., Guo, B. J., & Xu, R. G. (2017). Comparative mapping and candidate gene analysis of SSIIa associated with grain amylopectin content in Barley (*Hordeum vulgare* L.). *Frontiers in Plant Science, 8*, 1531. https://doi.org/10.3389/fpls.2017.01531

Fontaine, T., D'Hulst, C., Maddelein, M. L., Routier, F., Pepin, T. M., Decq, A., … Bossu, J. P. (1993). Toward an understanding of the biogenesis of the starch granule. Evidence that Chlamydomonas soluble starch synthase II controls the synthesis of intermediate size glucans of amylopectin. *Journal of Biological Chemistry, 268*(22), 16223–16230. https://doi.org/10.1016/0006-291X (60)90053-X

Fuwa, H., Inouchi, N., Glover, D. V., Fujita, S., Sugihara, M., Yoshioka, S., … Sugimoto, Y. (1999). Structural and physicochemical properties of endosperm starches possessing different alleles at the amylose-extender and waxy locus in Maize (*Zea mays* L.). *Starch, 51*(5), 147–151. https://doi.org/10.1002/(SICI)1521-379X(199905)51:5<147::AID-STAR147>3.0.CO;2-7

Hinchliffe, A., & Harwood, W. (2019). Agrobacterium-mediated transformation of barley immature embryos. In D. E. Briggs (Ed.), *Barley* (pp. 115–126). New York: Humana Press.

Huang, L. C., Li, Q. F., Zhang, C. Q., Chu, R., Gu, Z. W., Tan, H. Y., … Liu, Q. Q. (2020). Creating novel Wx alleles with fine-tuned amylose levels and improved grain quality in rice by promoter editing using CRISPR/Cas9 system. *Plant Biotechnology Journal, 18*(11), 2164–2166. https://doi.org/10.1111/pbi.13391

James, M. G., Denyer, K., & Myers, A. M. (2003). Starch synthesis in the cereal endosperm. *Current Opinion in Plant Biology, 6*(3), 215–222. https://doi.org/10.1016/S1369-5266(03)00042-6

Jane, J., Chen, Y. Y., Lee, L. F., McPherson, A. E., Wong, K. S., Radosavljevic, M., & Kasemsuwan, T. (1999). Effects of amylopectin branch chain length and amylose content on the gelatinization and pasting properties of starch. *Cereal Chemistry, 76*, 629–637. https://doi.org/10.1094/CCHEM.1999.76.5.629

Jane, J., Maningat, C. C., & Wongsagonsup, R. (2010). Starch characterisation, variety and application. In *Industrial crops and uses* (pp. 207–235). https://doi.org/10.1079/9781845936167.0207

Krueger, B. R., Walker, C. E., Knutson, C. A., & Inglett, G. E. (1987). Differential scanning calorimetry of raw and annealed starch isolated from normal and mutant maize genotypes. *Cereal Chemistry, 64*, 187–190. https://doi.org/10.1007/BF01027750

Lawrenson, T., Shorinola, O., Stacey, N., Li, C. D., Østergaard, L., Patron, N., Uauy, C., & Harwood, W. (2015). Induction of targeted, heritable mutations in barley and *Brassica oleracea* using RNA-guided Cas9 nuclease. *Genome Biology, 16*(1), 1–13. https://doi.org/10.1186/s13059-015-0826-7

Li, C. Y., Zhou, D. D., Fan, T., Wang, M. Y., Zhu, M., Ding, J. F., … Shi, Y. C. (2020). Structure and physicochemical properties of two waxy wheat starches. *Food Chemistry, 318*, Article 126492. https://doi.org/10.1016/j.foodchem.2020.126492

Li, H., Prakash, S., Nicholson, T. M., Fitzgerald, M. A., & Gilbert, R. G. (2016). The importance of amylose and amylopectin fine structure for textural properties of cooked rice grains. *Food Chemistry, 196*, 702–711. https://doi.org/10.1016/j.foodchem.2015.09.112

Li, J. Y., Jiao, G. A., Sun, Y. W., Chen, J., Zhong, Y. X., Yan, L., Jiang, D., Ma, Y. Z., & Xia, L. Q. (2021). Modification of starch composition, structure and properties through editing of TaSBEIIa in both winter and spring wheat varieties by CRISPR/Cas9. *Plant Biotechnology Journal, 19*(5), 937–951. https://doi.org/10.1111/pbi.13519

Li, Z. Y., Li, D. H., Du, X. H., Wang, H., Larroque, O., Jenkins, C. L. D., … Morell, M. K. (2011). The barley amo 1 locus is tightly linked to the starch synthase IIIa gene and negatively regulates expression of granule-bound starch synthetic genes. *Journal of Experimental Botany, 62*(14), 5217–5231. https://doi.org/10.1093/jxb/err239

Luo, J. X., Ahmed, R., Kosar-Hashemi, B., Larroque, O., Butardo, V. M., Tanner, G. J., … Li, Z. Y. (2015). The different effects of starch synthase IIa mutations or variation on endosperm amylose content of barley, wheat and rice are determined by the distribution of starch synthase I and starch branching enzyme IIb between the starch granule and amyloplast stroma. *Theoretical and Applied Genetics, 128*(7), 1407–1419. https://doi.org/10.1007/s00122-015-2515-z

Morell, M. K., Kosar-Hashemi, B., Cmiel, M., Samuel, M. S., Chandler, P., Rahman, S., … Li, Z. Y. (2003). Barley sex6 mutants lack starch synthase IIa activity and contain a starch with novel properties. *Plant Journal, 34*(2), 173–185. https://doi.org/10.1046/j.1365-313x.2003.01712.x

Nelson, O. E., & Rines, H. W. (1962). The enzymatic deficiency in the waxy mutant of maize. *Biochemical and Biophysical Research Communications, 9*, 297–300. https://doi.org/10.1016/0006-291X(62)90043-8

Panyoo, A. E., & Emmambux, M. N. (2017). Amylose–lipid complex production and potential health benefits: A mini-review. *Starch, 69*, 7–8. https://doi.org/10.1002/star.201600203

Regina, A., Bird, A., Topping, D., Bowden, S., Freeman, J., Barsby, T., Kosar-Hashemi, B., Li, Z. Y., Sadequr Rahman, S., & Morell, M. (2006). High-amylose wheat generated by RNA interference improves indices of large-bowel health in rats. *Proceedings of the National Academy of Sciences of the United States of America, 103*, 3546–3551. www.pnas.org/cgi/doi/10.1073/pnas.0510737103.

Regina, A., Kosar-Hashemi, B., Ling, S., Li, Z. Y., Rahman, S., & Morell, M. (2010). Control of starch branching in barley defined through differential RNAi suppression of starch branching enzyme IIa and IIb. *Journal of Experimental Botany, 61*(5), 1469–1482. https://doi.org/10.1093/jxb/erq011

Schultz, J., Copley, R. R., Doerks, T., Ponting, C. P., & Bork, P. (2000). SMART: A web-based tool for the study of genetically mobile domains. *Nucleic Acids Research, 28*(1), 231–234. https://doi.org/10.1046/j.1365-313X.2003.01712.x

South, J. B., & Morrison, W. R. (1990). Isolation and analysis of starch from single kernels of wheat and barley. *12*(1), 43–51. https://doi.org/10.1016/S0733-5210(09)80156-2

Sun, C., Sathish, P., Ahlandsberg, S., & Jansson, C. (1998). The two genes encoding starch-branching enzymes IIa and IIb are differentially expressed in barley. *Plant Physiology, 118*(1), 37–49. https://doi.org/10.2307/4278422

Topping, D. L., Morell, M. K., King, R. A., Li, Z., Bird, A. R., & Noakes, M. (2003). Resistant starch and health – Himalaya 292, a novel barley cultivar to deliver benefits to consumers. *Starch, 55*, 539–545. https://doi.org/10.1002/star.200300221

Umemoto, T., Aoki, N., Lin, H. X., Nakamura, Y., Inouchi, N., Sato, Y., Yano, M., Hirabayashi, H., & Maruyama, S. (2004). Natural variation in rice starch synthase IIa affects enzyme and starch properties. *Functional Plant Biology, 31*(7), 671–684. https://doi.org/10.1071/FP04009

Wang, X. C., Li, X. F., Deng, X., Han, H. P., Shi, W. L., & Li, Y. X. (2007). A protein extraction method compatible with proteomic analysis for the euhalophyte *Salicornia europaea*. *Electrophoresis, 28*(21), 3976–3987. https://doi.org/10.1002/elps.200600805

Wei, C. X., Xu, B., Qin, F. L., Yu, H. G., Chen, C., Meng, X., Zhu, L., Wang, Y. P., Gu, M. H., & Liu, Q. Q. (2010). C-type starch from high-amylose rice resistant starch granules modified by antisense RNA inhibition of starch branching enzyme. *Journal of Agricultural and Food Chemistry, 58*(12), 7383–7388. https://doi.org/10.1021/jf100385m

Xu, Y., Lin, Q. P., Li, X. F., Wang, F. Q., Chen, Z. H., Wang, J., Li, W. Q., Fan, F. J., Tao, Y. J., Jiang, Y. J., Wei, X. D., Zhang, R., Zhu, Q. H., Bu, Q. Y., Yang, J., & Gao, C. X. (2021). Fine-tuning the amylose content of rice by precise base editing of the Wx gene. *Plant Biotechnology Journal, 19*(1), 11. https://doi.org/10.1111/pbi.13433

Yamamori, M., Fujita, S., Hayakawa, K., Matsuki, J., & Yasui, T. (2000). Genetic elimination of a starch granule protein, SGP-1, of wheat generates an altered starch with apparent high amylose. *Theoretical and Applied Genetics, 101*(1–2), 21–29. https://doi.org/10.1007/s001220051444

Yamamori, M., Nakamura, T., Endo, T., & Nagamine, T. (1994). Waxy protein deficiency and chromosomal location of coding genes in common wheat. *Theoretical and Applied Genetics, 89*(2–3), 179–184. https://doi.org/10.1007/BF00225138

Yan, L., Fairclough, R., & Bhave, M. (2000). A novel starch granule-bound protein in endosperm of wheat. *Journal of Cereal Science, 32*(3), 245–258. https://doi.org/10.1006/jcrs.2000.0335

Yang, Q., Li, S. Y., Li, X. Y., Ma, J., Wang, J. R., Qi, P. F., … Jiang, Q. T. (2019). Expression of the high molecular weight glutenin 1Ay gene from *Triticum urartu* in barley. *Transgenic Research, 28*(2), 225–235. https://doi.org/10.1007/s11248-019-00117-6

Yang, Q., Zhong, X. J., Li, Q., Lan, J. Y., Tang, H. P., Qi, P. F., … Jiang, Q. T. (2020). Mutation of the d-hordein gene by RNA-guided Cas9 targeted editing reducing the grain size and changing grain compositions in barley. *Food Chemistry, 311*, Article 125892. https://doi.org/10.1016/j.foodchem.2019.125892

Zeng, D. C., Liu, T. L., Ma, X. L., Wang, B., Zheng, Z. Y., Zhang, Y. L., Xie, X. R., Yang, B. W., Zhao, Z., Zhu, Q. L., & Liu, Y. G. (2020). Quantitative regulation of Waxy expression by CRISPR/Cas9-based promoter and 5′UTR-intron editing improves grain quality in rice. *Plant Biotechnology Journal, 18*(12), 2385–2387. https://doi.org/10.1111/pbi.13427

Zhang, X., Colleoni, C., Ratushna, V., Sirghie-Colleoni, M., James, M., & Myers, A. M. (2004). Molecular characterization demonstrates that the *Zea mays* gene sugary2 codes for the starch synthase isoform SSIIa. *Plant Molecular Biology, 54*(6), 865–879. https://doi.org/10.1007/s11103-004-0312-1

Zhu, F. (2017). Barley starch: Composition, structure, properties, and modifications. *Comprehensive Reviews in Food Science and Food Safety, 16*(4), 558–579. https://doi.org/10.1111/1541-4337.12265